Taylor & Francis
Taylor & Francis Group

Journal of Toxicology and Environmental Health, Part B
Critical Reviews

ISSN: (Print) (Online) Journal homepage: https://www.tandfonline.com/loi/uteb20

Additive Manufacturing for Occupational Hygiene: A Comprehensive Review of Processes, Emissions, & Exposures

A.B. Stefaniak, S Du Preez & JL Du Plessis

To cite this article: A.B. Stefaniak, S Du Preez & JL Du Plessis (2021) Additive Manufacturing for Occupational Hygiene: A Comprehensive Review of Processes, Emissions, & Exposures, Journal of Toxicology and Environmental Health, Part B, 24:5, 173-222, DOI: 10.1080/10937404.2021.1936319

To link to this article: https://doi.org/10.1080/10937404.2021.1936319

Published online: 17 Jun 2021.

JOURNAL OF TOXICOLOGY AND ENVIRONMENTAL HEALTH, PART B
2021, VOL. 24, NO. 5, 173–222
https://doi.org/10.1080/10937404.2021.1936319

Taylor & Francis
Taylor & Francis Group

Additive Manufacturing for Occupational Hygiene: A Comprehensive Review of Processes, Emissions, & Exposures

A.B. Stefaniak[a†], S Du Preez[b], and JL Du Plessis[b]

[a]Respiratory Health Division, National Institute for Occupational Safety and Health, Morgantown, WV, USA; [b]North-West University, Occupational Hygiene and Health Research Initiative, Potchefstroom, South Africa

ABSTRACT

This comprehensive review introduces occupational (industrial) hygienists and toxicologists to the seven basic additive manufacturing (AM) process categories. Forty-six articles were identified that reported real-world measurements for all AM processes, except sheet lamination. Particles released from powder bed fusion (PBF), material jetting (MJ), material extrusion (ME), and directed energy deposition (DED) processes exhibited nanoscale to submicron scale; real-time particle number (mobility sizers, condensation nuclei counters, miniDiSC, electrical diffusion batteries) and surface area monitors (diffusion chargers) were generally sufficient for these processes. Binder jetting (BJ) machines released particles up to 8.5 µm; optical particle sizers (number) and laser scattering photometers (mass) were sufficient for this process. PBF and DED processes (powdered metallic feedstocks) released particles that contained respiratory irritants (chromium, molybdenum), central nervous system toxicants (manganese), and carcinogens (nickel). All process categories, except those that use metallic feedstocks, released organic gases, including (but not limited to), respiratory irritants (toluene, xylenes), asthmagens (methyl methacrylate, styrene), and carcinogens (benzene, formaldehyde, acetaldehyde). Real-time photoionization detectors for total volatile organics provided useful information for processes that utilize polymer feedstock materials. More research is needed to understand 1) facility-, machine-, and feedstock-related factors that influence emissions and exposures, 2) dermal exposure and biological burden, and 3) task-based exposures. Harmonized emissions monitoring and exposure assessment approaches are needed to facilitate inter-comparison of study results. Improved understanding of AM process emissions and exposures is needed for hygienists to ensure appropriate health and safety conditions for workers and for toxicologists to design experimental protocols that accurately mimic real-world exposure conditions.

KEYWORDS

Process descriptions; 3D printing; particles; gases; monitoring; research needs

ABBREVIATIONS ABS : acrylonitrile butadiene styrene; ACGIH® TLV® : American Conference of Governmental Industrial Hygienists Threshold Limit Value; ACH : air change per hour; AM : additive manufacturing; ASA : acrylonitrile styrene acrylate; AVP : acetone vapor polishing; BJ : binder jetting; CAM-LEM : computer-aided manufacturing of laminated engineering materials; CNF : carbon nanofiber; CNT : carbon nanotube; CP : co-polyester; CNC : condensation nuclei counter; CVP : chloroform vapor polishing; DED : directed energy deposition; DLP : digital light processing; EBM : electron beam melting; EELS : electron energy loss spectrometry; EDB : electrical diffusion batteries; EDX : energy dispersive x-ray analyzer; ER : emission rate; FDM™ : fused deposition modeling; FFF : fused filament fabrication; IAQ : indoor air quality; LSP : laser scattering photometer; LCD : liquid crystal display; LDSA : lung deposited particle surface area; LOD : limit of detection; LOM : laminated object manufacturing; LOQ : limit of quantitation; MCE : mixed cellulose ester filter; ME : material extrusion; MJ : material jetting; OEL : occupational exposure limit; OPS : optical particle sizer; PBF : powder bed fusion; PBZ : personal breathing zone; PC : polycarbonate; PEEK : poly ether ether ketone; PET : polyethylene terephthalate; PETG : Polyethylene terephthalate glycol; PID : photoionization detector; PLA : polylactic acid; PM_1 : particulate matter with aerodynamic diameter less than 1 µm; $PM_{2.5}$: particulate matter with aerodynamic diameter less than 2.5 µm; PM_{10} : particulate matter with aerodynamic diameter less than 10 µm; PSL : plastic sheet lamination; PVA : polyvinyl alcohol; REL : recommended exposure limit; SDL : selective deposition lamination; SDS : safety data sheet; SEM : scanning electron microscopy; SL : sheet lamination; SLA : stereolithography; SLM : selective laser melting; SMPS : scanning mobility particle sizer; SVOC : semi-volatile organic compound; TEM : transmission electron microscopy; TGA : thermal gravimetric analysis; TPU : thermo polyurethane; UAM : ultrasonic additive manufacturing; UC : ultrasonic consolidation; TVOC : total volatile organic compounds; TWA : time-weighted average; VOC : volatile organic compound; VP : vat photopolymerization

CONTACT A.B. Stefaniak AStefaniak@cdc.gov Respiratory Health Division, National Institute for Occupational Safety and Health, 1095 Willowdale Road, Morgantown, WV, 26505, USA

[†]Author to whom correspondence should be sent

Introduction

Additive manufacturing (AM) is the process of joining feedstock materials to make parts from a computer file (ISO/ASTM 2015). Parts made by AM are usually built using layer-upon-layer addition of feedstock material, which differs from traditional subtractive manufacturing where material is selectively removed to make a part or formative manufacturing methodologies where material is forged or molded to make a part. AM has been used for rapid prototyping and manufacturing since the early 1990s (Bourell 2016).

In 2004, a case of allergic dermatitis was reported in a worker who operated a vat photopolymerization machine (Chang et al. 2004), which to our knowledge was the first report of an adverse health effect associated with an AM exposure. When key patents on fused deposition modeling (FDM™) material extrusion machines expired in 2005, there was a surge in availability of low-cost machines that utilize fused filament fabrication (FFF) technology, what is now commonly referred to as 3D printers (Ford 2014). AM is colloquially referred to as 3D printing; however, these are technically different. The term 3D printing has generally referred to machines that were low end in price and/or capability (ISO/ASTM 2015), most commonly those based on FFF technology, which is one variation of the material extrusion AM process category.

The availability of low-cost FFF 3D printers has led to a rise in their use for various industrial applications as well as in offices, classrooms, libraries, homes, and other non-industrial spaces. Stephens et al. first reported that FFF 3D printers emitted ultrafine particles (diameter < 100 nm) at rates that exceeded 10 billion particles/min in an office space (Stephens et al. 2013), which brought AM to the widespread attention of the occupational (industrial) hygiene community and set off a cascade of research on the topic. Though AM is gaining popularity in many industries (Ford 2014; Wu et al. 2020), some occupational (industrial) hygienists and toxicologists may not be familiar with all types of AM process categories and the substances released from these processes. Further, approaches to measure substances that are released into indoor air need clarification for appropriate selection of measurement methods for exposure assessments. Identification of appropriate measurement methods is also needed for design of toxicology studies to ensure exposures are based on real-world exposure conditions. Hence, the purposes of this comprehensive review were to: 1) introduce occupational (industrial) hygienists and toxicologists to the seven basic AM process categories, 2) summarize available data on substances that are released from each of these process categories, 3) critically evaluate approaches used to characterize releases (emission rates [ERs] and concentrations), and 4) identify research needs to more fully understand emissions and exposures.

Additive manufacturing process categories

Based on internationally harmonized terminology, there are seven basic AM process categories:

- binder jetting (BJ) – a liquid bonding agent is selectively deposited to join powder,
- directed energy deposition (DED) – focused thermal energy is used to fuse materials via melting as they are deposited,
- material extrusion (ME) – material is selectively dispensed through a nozzle or orifice,
- material jetting (MJ) – droplets of build material are selectively deposited,
- powder bed fusion (PBF) – thermal energy selectively fuses regions of a powder bed,
- sheet lamination (SL) – sheets of material are bonded to form a part, and
- vat photopolymerization (VP) – liquid photopolymer in a vat is selectively cured by light-activated polymerization (ISO/ASTM 2015).

An AM system consists of a machine and associated equipment needed to manufacture a part. Within an AM system, the build chamber is the location where the part is made and it is often, but not always, enclosed. Historically, the purpose of an enclosed build chamber was to maintain necessary conditions during a build cycle (e.g., atmospheric thermal stability). Some manufacturers now sell enclosed AM systems with filters intended for exposure mitigation (Katz et al. 2020). Within the

build chamber, parts are built on a build platform, which depending on the process may be positioned in a horizontal or vertical orientation and may or may not be heated. For DED, ME, MJ, SL, and VP the part is built attached to the build platform (directly or via support material) whereas in BJ and PBF the part is built in a powder bed and is not fixed to the build platform (ISO/ASTM 2015).

All AM parts are built from feedstock, which is the building material supplied to an AM process. As summarized in Table 1, feedstock may be in the form of solid powder, filaments, pellets and sheets or liquid resins. Some feedstock materials contain wood, metals, clays, carbon or glass fibers, ceramics, engineered nanomaterials, flame retardants or other additives and fillers for functional or esthetic purposes (Ivanova, Williams, and Campbell 2013; Wu et al. 2020).

Binder jetting

From Figure 1(a), the basic operating principle of a binder jetting machine is as follows: 1) a blade spreads a thin layer of powder over the build platform, 2) a carriage with nozzles selectively deposits droplets of a binder in a pattern onto the powder to bond the particles together via a chemical reaction, 3) the powder bed is lowered incrementally and the blade spreads a fresh layer of powder on top of the hardened powder, 4) binder is again selectively deposited onto the powder bed and hardens the next layer of particles, and 5) the process is repeated until the final build cycle is built (Afshar-Mohajer et al. 2015). The final part is submerged in a powder "cake" and is recovered manually. For some machines, the feedstock powder and a liquid activator are mixed, and the binder is applied to the mixture to harden the material, whereas in others an activator and binder are mixed then sprayed onto the powder to harden the material. For this AM process category, pre-printing tasks include loading powder in the machine, post-printing tasks include opening machine doors and de-powdering printed parts, and post-processing might include spray coating of printed parts.

Table 1. Physical and chemical characteristics of AM process feedstock materials. Adapted from cit.(ISO/ASTM 2015; Wu et al. 2020).

Process	Physical state	Chemical composition
Binder jetting	Solid powder	Polymers, metals, ceramics, composites
Directed energy deposition	Solid wire	Metals
Material extrusion	Solid filament or pellets	Thermopolymers[a]
Material jetting	Liquid resin	Photopolymers[a]
Powder bed fusion	Solid powder	Polymers, metals, ceramics, composites, glasses
Sheet lamination	Solid layers	Polymers, metals, ceramics, composites, papers
Vat photopolymerization		
Liquid resin	Photopolymers[a]	

[a]May contain metals, ceramics, composites, nanomaterials, or other additives

Directed energy deposition

In DED, the focused thermal energy source is a laser, electron beam, plasma, or electric arc. Feedstock materials are either in wire or powder form. From Figure 1(b), for wire, the feedstock is 1) fed into the path of the thermal energy source, where it 2) melts and drips onto the build platform in a molten pool and cools and hardens to form a shape. For powder, the feedstock is dispensed via a nozzle. The outer ring of the nozzle dispenses the powder and the inner ring is a laser, which melts the powder and sprays it onto the build platform. For flammable metal powders such as titanium, an inert atmosphere must be maintained in the build chamber (e.g., kept under vacuum or purged with nitrogen or argon gas or local inert gas shielding at the build platform similar to welding) and the AM machine must be properly bonded and grounded to prevent oxidation and fire (Bau et al. 2020). For DED, pre-printing tasks include loading wire or powder into the machine, post-printing tasks include opening machine doors to retrieving printed parts and cutting parts from the build platform, and post-processing can include machining operations to achieve final part dimensions.

Material extrusion

From Figure 1(c), solid polymer is 1) heated to just above its glass transition temperature and dispensed on a build platform, 2) layer-upon-layer to build a part. Numerous polymers are commercially available for ME, and each has unique properties such as thermal stability and chemical resistance (Wu et al. 2020). Variations of ME include fused deposition modeling (FDM™), a technique created and trademarked by Stratasys Inc., FFF, and large

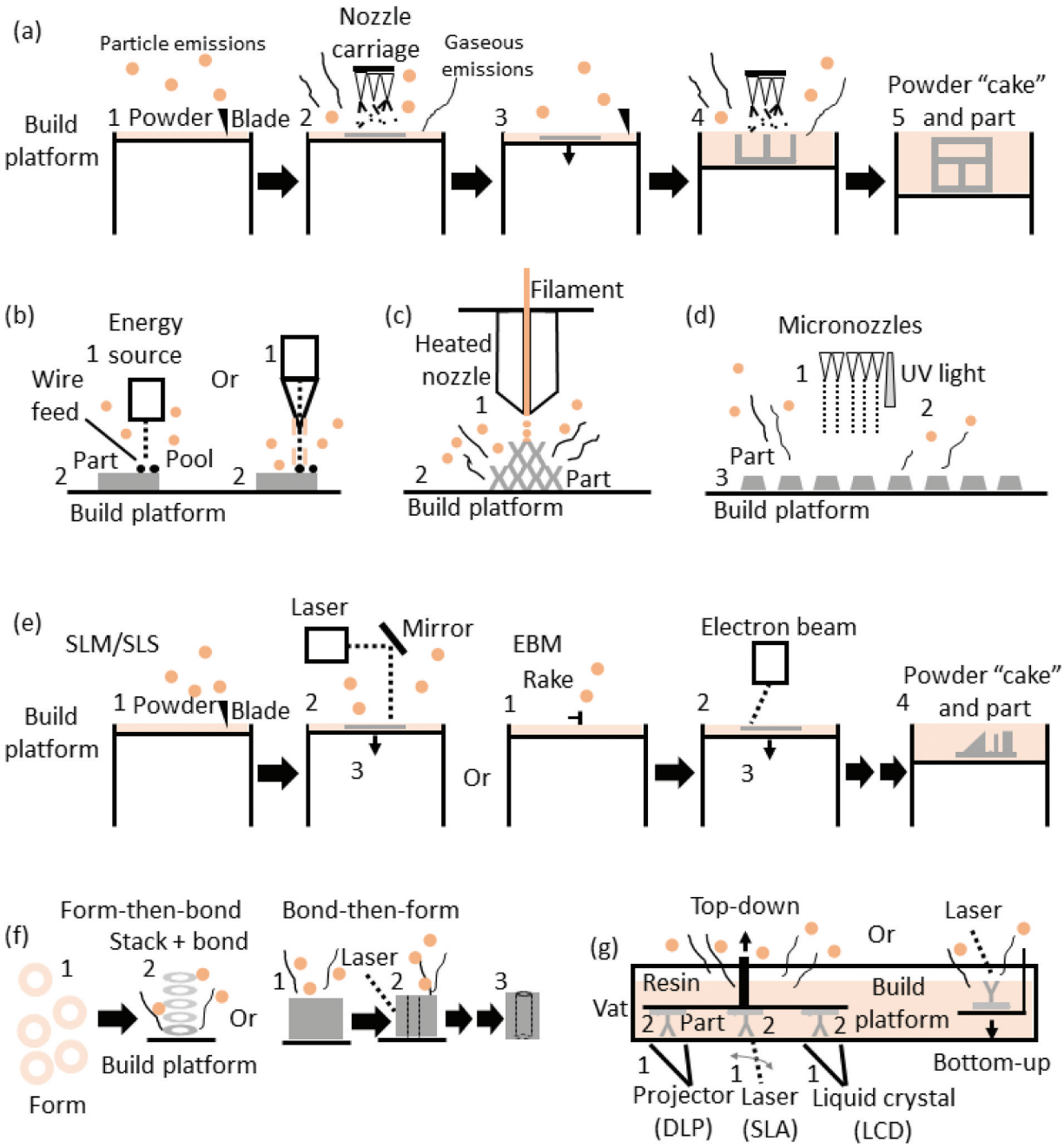

Figure 1. Principles of additive manufacturing processes: (a) binder jetting, (b) directed energy deposition, (c) material extrusion, (d) material jetting, (e) powder bed fusion, (f) sheet lamination, and (g) vat photopolymerization. Numbers correspond to process steps given in the section on additive manufacturing process categories.

format additive manufacturing machines. Though FDM™ and FFF are similar, FDM™ generally refers to industrial-scale machines with enclosed heated build chambers, whereas FFF refers to lower cost desktop-scale ME-type 3-D printers (Bourell 2016; Ford 2014). FFF 3D printers with modified extruder nozzles are used for bioprinting with cells to create 3D tissue models for pre-clinical medical research, pharmaceutical drug discovery, and toxicity testing, e.g., screening of chemicals for irritancy (Ma et al. 2018; Shahin-Shamsabadi and Selvaganapathy 2019; Wei et al. 2020). Pre-printing tasks include loading polymer into machines as filament or pellets, post-printing tasks include opening machine doors to retrieve printed parts, and examples of post-processing tasks are acetone vapor polishing (AVP) and

chloroform vapor polishing (CVP) and sanding printed parts.

Material jetting

For MJ, liquid photopolymer resin is 1) dispensed onto a build platform via hundreds of micronozzles, 2) cured using an ultraviolet laser, and 3) the process repeated layer-by-layer to build a part (Figure 1(d)). Numerous resins are available commercially in a range of colors without and with additives that impart specific properties such as flexibility, surface appearance, etc. Pre-printing tasks include loading resin containers into the machine (exposures are expected to be low since most machines use a sealed container loading system), post-printing involves removing printed parts from the build platform, and post-processing usually includes washing (sometimes with ultrasound treatment) by submerging the part in water, followed by rinsing in a caustic bath.

Powder bed fusion

As shown in Figure 1(e), there are two main types of PBF processes, selective laser melting (SLM) that uses as a laser as the energy source and electron beam melting (EBM) that uses an electron beam as the energy source (Zhang et al. 2018). Historically, PBF was referred to as selective laser sintering (SLS), though this term is incorrect because the powder feedstock is fully or partially melted, not sintered (which involves using a mold and heat and/or pressure) (ISO/ASTM 2015). For SLM/SLS: 1) a blade spreads a thin layer of powder over the build platform, 2) a laser is reflected onto the powder using a mirror and it is selectively melted, 3) the powder bed is lowered incrementally and the blade spreads a fresh layer of powder on top of the previously hardened surface, and 4) the process is repeated until the final build cycle is complete. In EBM, a high-powered electron beam selectively melts powder feedstock under near-vacuum conditions: 1) a rake pushes a layer of powder over the build platform, 2) an electron beam is focused using a lens system and selectively melts the powder, 3) the powder bed is lowered incrementally and the rake pushes a fresh layer of powder on top of the previously hardened surface, and 4) the process is repeated until the final object is built (Wu et al. 2020). Upon completion of the final build cycle, the part is encased in powder (referred to as a "cake") and must be recovered manually. An inert atmosphere must be maintained in the build chamber and the AM machine must be properly bonded and grounded to prevent oxidation of feedstock powder. Examples of PBF pre-printing tasks include powder weighing, mixing, and loading into the machine. Examples of post-printing tasks are opening the machine to retrieve a printed part, de-powdering (e.g., vacuuming) excess powder from the build platform, removing the build platform with attached printed part from the machine, and sieving used powder and refilling the machine. Post-processing tasks include cutting the printed part from the build platform and grinding.

Sheet lamination

In SL, a single 2-dimensional layer of feedstock material is placed on a build platform (also called a cutting bed for this process) and successive layers are added until the final build cycle is complete (Figure 1(f)). Feedstock materials include 2-dimensional sheets of paper or polymer, ceramic tape, and metal in the form of tape, films, or ribbons. Variations of SL include computer-aided manufacturing of laminated engineering materials (CAM-LEM), laminated object manufacturing (LOM), plastic sheet lamination (PSL), selective deposition lamination (SDL), ultrasonic additive manufacturing (UAM), and ultrasonic consolidation (UC). These techniques differ in how they form and bond layers and are generally categorized as "form-then-bond" processes where, as shown in Figure 1 (f), the 1) feedstock is cut to shape (pre-printing task), 2) then bonded to the previous layer (printing task) to 3) form a part (e.g., CAM-LEM) and "bond-then-form" processes where 1) feedstock is bonded (printing task), 2) then cut using a laser or blade or by milling during the build or after the last build cycle (post-processing) to 3) form a part (e.g., SDL, UAM, UC). The technique used to bond layers of feedstock vary and include adhesives (e.g., LOM, SDL, PSL) and ultrasonic welding (UAM).

Vat photopolymerization

The main components of photopolymer resin for VP printers are binders, monomers, and photoinitiators (Wu et al. 2020). As shown in Figure 1(g), variations of VP technology include, but are not limited to, stereolithography (SLA), digital light processing (DLP), and liquid crystal display (LCD) (Wu et al. 2020; Zhang et al. 2018). SLA printers 1) scan a laser beam across the print area to 2) selectively cure resin on the bottom of a vat as series of points and rounded lines to build objects. DLP printers 1) use a high-resolution projector to flash black and white image slices of each object layer across the entire bottom surface of the vat at once, the projector is a digital screen that forms white areas of the projected image made of square pixels that are 2) cured using UV or multi-wavelength light from a lamp to build a part (Wu et al. 2020). LCD printers are similar to DLP technology, in that they 1) also flash complete layers at the resin on the bottom surface of the vat; however, the light source is UV light from an array of light-emitting diodes shining through a liquid crystal display not a projector and 2) a screen is used as a mask that reveals only the pixels necessary for the current layer to be hardened. VP machines either use a "top-down" or "bottom-up" approach to build a part, though the former is more common (Wu et al. 2020). In "top-down" machines: 1) the build platform is lowered into the vat until it almost touches the bottom of the reservoir, leaving a thin layer of resin between the platform and vat, 2) a light source is aimed up at the build platform and hardens the resin, 3) the platform is incrementally raised to allow a new layer of resin to fill the gap between the platform and bottom of the vat, and 4) the light source hardens the new layer of resin and the process repeated until the last build cycle is complete (Wu et al. 2020; Zhang et al. 2018). In the bottom-up approach: 1) a build platform is submerged just below the surface of the resin in a vat, 2) a light source is aimed down at the build platform and hardens the resin, 3) the platform is incrementally lowered and a roller pushes a new layer of resin across the previously hardened layer, and 4) the light source hardens the new layer of resin and the process repeated until the last build cycle is complete. Regardless of approach, the first solidified layer is attached to the build platform not the vat surface. For all variations of VP, pre-printing tasks include mixing and dispensing resin into vats (can be done outside of the machine or inside the machine) and/or loading a pre-filled vat into the machine. Post-printing tasks include opening the machine to retrieve the printed part, UV-curing to harden unreacted monomers, and ethanol cleaning to remove resin from part surfaces. Post-processing tasks can include sanding and drilling of the manufactured part.

General occupational hygiene considerations

AM applications and uses are rapidly growing; however, to date only a few publications have addressed worker safety and health. Deak (1999) first expressed the need for safe work practices in rapid prototyping laboratories and raised concerns over exposure to novel materials (chemicals), repeated exposure (sensitivity leading to allergic reactions), and potential long-term effects of exposures. Later, Short et al. (2015) performed risk assessments and hazard identification for three AM process categories (ME, BJ, and VP) and identified contact with toxic chemicals (ranging from carcinogens to mucous membrane irritants), use of flammable and explosive materials (e.g. metal dusts), and irradiation of the eyes (UV radiation and lasers) as major potential hazards. Ryan and Hubbard (2016) reported a preliminary hazard assessment for MJ process category. Recently, Petretta et al. (2019) constructed a risk evaluation system for all AM process categories except SL. All AM processes present some form of hazard to workers; however, the potential for exposure varies among the seven categories (Bours et al. 2017; Petretta et al. 2019; Roth et al. 2019), as well as within process phases and the operating environment (Roth et al. 2019). Inhalation of particles (including ultrafine particles) and semi- and volatile organic compound (SVOC, VOC) emissions, dermal exposure to binders, powders, resins, and solvents and UV radiation are now considered to be among the most important health hazards associated with AM (Petretta et al. 2019; Roth et al. 2019). In particular, exposures to ultrafine particles (diameter < 100 nm) pose a challenge for

occupational hygienists who are accustomed to mass-based exposure measurements. Ultrafine particles, because of their small size, have little mass and thus characterized in terms of number concentration. Exposure to ultrafine particles was shown to induce adverse cardiovascular effects (e.g., hypertension) in humans and experimental animals. Further, because of their small size, these particles can penetrate to the deepest portion of the lung and translocate to extrapulmonary sites where they can induce toxic effects (Elder and Oberdörster 2006). At this time, there are no particle number-based occupational exposure limits (OELs) so hygienists and toxicologists have no standard against which measurements can be compared to determine if exposures are acceptable or unacceptable. Some investigators characterized FFF 3D printer particle number-based ERs as low ($< 10^9$ #/min), medium (10^9 #/min), and high ($> 10^9$ #/min) using criteria developed by He, Morawska, and Taplin (2007) for laser printers; however, these classifications are not related to health risks. Additional hazards of AM include electrical shock, thermal burns, mechanical injury (during maintenance and malfunction), noise, contact with biological agents (e.g., 3D bioprinting), fatigue (long shift durations), psychosocial stress, and repetitive manual tasks (ergonomics/human factors) (Petretta et al. 2019; Roth et al. 2019).

Exposures need to be controlled via the hierarchy of controls, which includes, but is not limited to proper facility and process design, ventilation and dust collection, adequate workspace, and, as a last resort, use of personal protective technologies such as respirators. Examples of effective controls for preventing or reducing exposures were described in the literature (Dunn et al. 2020b; Katz et al. 2020; Pelley 2018; Petretta et al. 2019; Roth et al. 2019).

Methods

The Scopus and PubMed databases were searched in July 2020 using the keywords (additive manufacturing OR 3-d print* OR 3-dimensional) AND (emissions OR exposure), which returned 888 and 416 citations, respectively. Each abstract was reviewed by one author to determine if the citation met the eligibility criteria for this review, i.e., available in English language and reported original data on substances released from an AM process into a workplace or other indoor space that could be occupied by a person (all environmental test chamber studies were excluded). Based upon these criteria, 27 of the 888 citations from Scopus and 12 of the 416 citations from PubMed were retained. These 39 citations were merged, and 8 duplicates were removed, which resulted in 31 candidate articles for detailed review. Next, both databases were searched using variations of AM process category and machine names. For example, for vat photopolymerization, the keywords were (vat printing OR SLA printing OR DLP printing OR LCD printing OR continuous liquid interface production OR low force stereolithography) AND (emissions OR exposure). These search queries identified an additional five citations that met our eligibility criteria and brought the total number of candidate articles to 36. All authors obtained these articles and reviewed them in detail. During this detailed review, an additional 6 articles that met our eligibility criteria were identified from citations in the articles, which raised the total to 42 articles. From the time of the initial literature review to December 31, 2020, four relevant articles were published electronically that were identified using a weekly key word search alert of the Scopus database, bringing the final total to 46 articles that were included in this review. Recently, Leso et al. (2021) reviewed 18 articles specific to workplace exposure assessments and discussed issues related to risk management and exposure mitigation and the reader is referred to that publication for more information on those topics.

AM process category emissions and associated exposures

Since the first publication on particle emissions from ME-type FFF 3-D printers in 2013 (Stephens et al. 2013), the number of articles related to emissions and exposures associated with AM published per year has increased and reached a maximum of 17 in 2019 (Figure 2). With time, studies on the various AM process categories have diversified beyond just the ME process category, with studies of five different AM process categories published in the last two years respectively. AM emissions and exposure articles included in this review originated

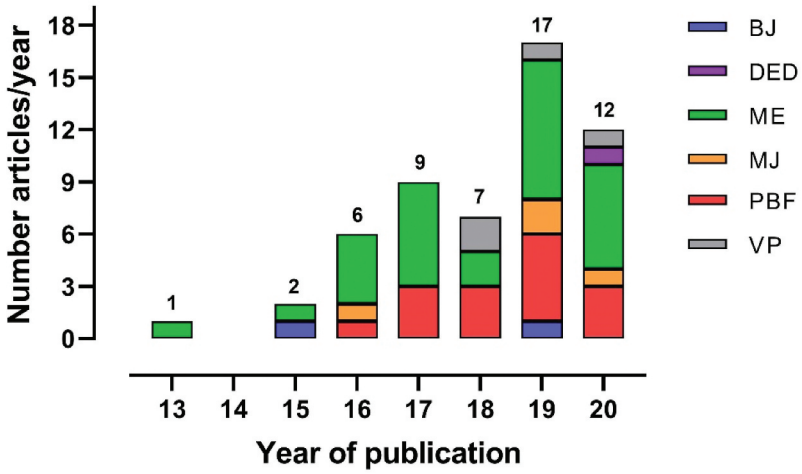

Figure 2. AM workspace emission and exposure articles published from 2013 to 2020 according to process categories and year of publication.

from 23 countries, which highlights the global impact of this technology and international efforts to ensure that proper health and safety precautions are implemented during use. The USA was responsible or involved in 46% of published articles and France, South Africa, Singapore, and Sweden were responsible or involved in 7% of published articles (Figure 3).

For the purposes of this review, the term emission was defined as any substance that was released from an AM process or associated task and the term exposures was defined as the amount of a substance that was measured in a person's breathing zone, on their skin, or in a biological fluid. Additional details on hazards associated with metallic feedstock used in AM processes have been published (Chen et al.

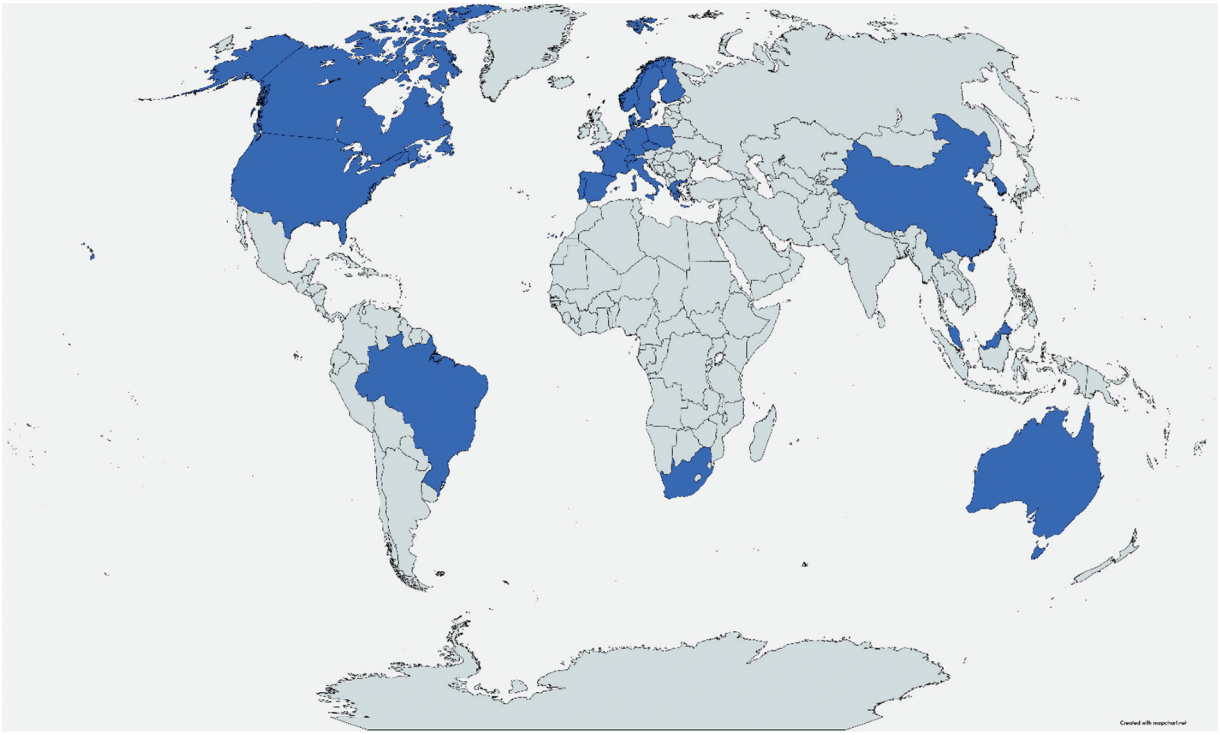

Figure 3. AM workspace emission and exposure articles according to countries of origin (drawn on mapchart.net).

2020; Sousa, Arezes, and Silva 2019) as were additional details on hazards specific to acrylonitrile butadiene styrene (ABS) and polylactic acid (PLA) filaments used in ME processes (Aluri et al. 2021). Literature on particle emissions and exposures are summarized in Tables 2 and 3, respectively. Gas-phase emissions and exposures are summarized in Tables 4 and 5, respectively. Several investigators reported comprehensive measurements for metals and/or VOCs; however, for brevity, only the top five substances by mass concentration from these studies were included in the tables. Emissions and exposures occur throughout the entire AM process, which includes pre-printing tasks (cleaning a build chamber, loading feedstock in a machine, etc.), printing, post-printing tasks (retrieving a printed part, unloading feedstock from a machine, etc.), and post-processing tasks (cleaning, polishing, machining and other manipulations of printed parts, etc.). Data presented herein are useful to occupational (industrial) hygienists for understanding exposure potential and to toxicologists for developing experimental protocols based on real-world data for *in vitro* and *in vivo* studies.

Binder jetting

Two publications focused on BJ process emissions, one using gypsum powder as the feedstock material and the other using stainless steel powder; each printer was housed in university research lab (157 m^3 room with two air exchanges per hour (ACH) and 70 m^3 room, ACH not reported, respectively). No personal exposure monitoring data were reported in the literature for BJ processes. Overall, particle number concentrations measured with a mobility sizer during printing were 1×10^4 to 3×10^4 #/cm^3 and total volatile organic compound (TVOC) concentrations reached 1725 μg/m^3 for the gypsum process and average particle number concentration was 7000 #/cm^3 for the stainless steel process (Afshar-Mohajer et al. 2015; Lewinski, Secondo, and Ferri 2019).

Afshar-Mohajer et al. (2015) performed real-time monitoring of airborne particles and TVOC concentrations for three different periods (before, during, and after printing with gypsum) and investigated the effect of opening the machine lid on workplace contaminant concentrations. From Table 2, during printing, particle number concentrations peaked at 0.9 to 1.2×10^4 #/cm^3 for the 205 to 255 nm size fraction; however, 54.3 nm sized particles were most evident at the beginning of printing. The highest number-based particle emission rate (ER) occurred when the top cover of the AM machine was opened after printing (approximately 4.4×10^4 #/min for the 305 to 407 nm size fraction). Particles with a size of 407 nm displayed the highest mass-based ER of approximately 0.9 ng/min. Particle emissions up to 8.5 μm in size were measured with an optical particle sizer (OPS) (Afshar-Mohajer et al. 2015). Lewinski, Secondo, and Ferri (2019) observed little to slight increased average particle number concentrations for 0.3 to 10 μm sized particles during printer setup (3.5×10^4 #/cm^3), printing (3.8×10^4 #/cm^3), and during post-print powder de-powdering with stainless steel (3.3×10^4 #/cm^3) compared with background (3.3×10^4 #/cm^3). Scanning mobility particle sizer (SMPS) data indicated that emission of 60 nm sized particles peaked approximately 30 min after the start of the printing process and reached a maximum of 7000 #/cm^3; however, the mean concentrations during background, printing, and de-powdering were similar (5900 #/cm^3). During printing concentrations total particulate mass collected on filters ranged from below the analytical limit of detection (LOD) to 80 μg/m^3 (corresponding to a particulate matter with aerodynamic size less than 2.5 μm ($PM_{2.5}$) concentration of 30 μg/m^3) within one m of the printer and 20 μg/m^3 at more than three m from the printer. The measured concentrations at 1 m from the printer did not differ from background, though the value measured at three m exceeded background (Lewinski, Secondo, and Ferri 2019).

For the gypsum powder BJ printer, TVOC concentration increased prior to printing (machine in standby mode). When the printer was turned on, TVOC concentration rose only slightly but particle number concentration increased rapidly (Table 4). Hence, the binder solution (cyanoacrylate and hydroquinone) in the storage tank of the printer emitted VOCs even when the printer was not operational. The highest TVOC concentration measured was 1725 μg/m^3 when the top cover was opened to remove the printed part (Afshar-Mohajer et al. 2015).

Table 2. Summary of particle-phase releases (emission rates and concentrations) from additive manufacturing machines by process category ($\bar{X}C_{num}$ = average particle number concentration in #/cm^3, ER_{num} = particle number-based emission rate in #/min, $\bar{X}C_{mass}$ = average particle mass concentration in µg/m^3).

Room (m^3)	ACH (h^{-1})	Feedstock[a]	Scenario[b]	Sampler[c]	Specifics[d]	$\bar{X}C_{num}$	ER_{num}	$\bar{X}C_{mass}$	Cit.[f]
Binder jetting AM process category									
157	6	Gypsum	Cover shut	CFC (TF)	TSP			400	A
				SMPS	205 nm	9000	4.4 x 10^4		
				SMPS	255 nm	1.2 x 10^4			
				SMPS	<407 nm	1 x 10^4–3 x 10^4			
				OPS	PM_1			680 (P)[e]	
				OPS	$PM_{2.5}$			58	
								800 (P)	
				OPS	PM_{10}			80	
								1100 (P)	
70	NR	SS	Printer setup	OPS	0.3 to 10 µm	3.5 x 10^4			B
			Printing	OPS	0.3 to 10 µm	3.8 x 10^4			
			Depowdering	OPS	0.3 to 10 µm	3.3 x 10^4			
			Printing	SMPS	27 to 65 nm	7000			
			1 m to printer	Impactor (TF)	$PM_{2.5}$			30	
			1 m to printer	CFC (TF)	PNOC			up to 80	
			3 m to printer	CFC (TF)	PNOC			20	
Directed energy deposition AM process category									
NR	NR	316 L SS, Inconel 625	Printing	CNC	10 to 1000 nm	0.5 x 10^6–1.5 x 10^6			C
		316 L SS	10VX nozzle	Inhal. (PVC)	Fe			124	
				Inhal. (PVC)	Cr			43.8	
				Inhal. (PVC)	Mn			14.2	
				Inhal. (PVC)	Ni			19.5	
				Inhal. (PVC)	Mo			6.8	
			10VX nozzle	Resp. (PVC)	Fe			61.7	
				Resp. (PVC)	Cr			30.9	
				Resp. (PVC)	Mn			14.5	
				Resp. (PVC)	Ni			8.0	
				Resp. (PVC)	Mo			<7.1	
		316 L SS	24 VX nozzle	Inhal. (PVC)	Fe			283	
				Inhal. (PVC)	Cr			110	
				Inhal. (PVC)	Mn			31.6	
				Inhal. (PVC)	Ni			42.2	
				Inhal. (PVC)	Mo			12.5	
				Resp. (PVC)	Fe			196	
				Resp. (PVC)	Cr			86.3	
				Resp. (PVC)	Mn			28.1	
				Resp. (PVC)	Ni			27.7	
				Resp. (PVC)	Mo			9.1	
		Inconel 625	10VX nozzle	Inhal. (PVC)	Fe			19.6	
				Inhal. (PVC)	Cr			86.3	
				Inhal. (PVC)	Mn			10.7	
				Inhal. (PVC)	Ni			92.2	
				Inhal. (PVC)	Mo			9.1	
				Resp. (PVC)	Cr			55.1	
				Resp. (PVC)	Mn			10.8	
				Resp. (PVC)	Ni			70.3	
				Resp. (PVC)	Mo			<9.0	

(*Continued*)

Table 2. (Continued).

Room (m^3)	ACH (h^{-1})	Feedstock[a]	Scenario[b]	Sampler[c]	Specifics[d]	$\bar{X}C_{num}$	ER_{num}	$\bar{X}C_{mass}$	Cit.[f]
		Inconel 625	24 VX nozzle	Inhal. (PVC)	Fe			44.7	
				Inhal. (PVC)	Cr			306	
				Inhal. (PVC)	Mn			45.0	
				Inhal. (PVC)	Ni			456	
				Inhal. (PVC)	Mo			77.7	
				Resp. (PVC)	Fe			28.0	
				Resp. (PVC)	Cr			261	
				Resp. (PVC)	Mn			44.6	
				Resp. (PVC)	Ni			346	
				Resp. (PVC)	Mo			66.4	
Material extrusion AM process category									
45	NR	PLA	3-DP	SMPS	10 to 116 nm	2.9×10^4	4.0×10^9		D
				SMPS	10 to 100 nm	2.8×10^4	2.0×10^{10}		
45	NR	ABS	3-DP	SMPS	10 to 116 nm		4.0×10^{10}		
				SMPS	10 to 100 nm		1.9×10^{11}		
60	NR	ABS	3-DP (n = 1)	OPS	250 to 280 nm	25 (P)			E
			3-DP (n = 2)	OPS	250 to 280 nm	40 (P)			
8	0.1	PLA	3-DP T_n = 180 to 220	CNC	2.5 to 1000 nm	0.3×10^5–4.5×10^5 (P)			F
			3-DP R_f = 30 to 90	CNC	2.5 to 1000 nm	5000–5200 (P)			
8	0.1	ABS	3-DP T_n = 200 to 240	CNC	2.5 to 1000 nm	0.3×10^5–2.7×10^5 (P)			
			3-DP R_f = 30 to 90	CNC	2.5 to 1000 nm	0.7×10^5–2.1×10^5 (P)			
28	NR	PLA	3-DP	CNC	20 to 1000 nm	1950		0.014*	G
544	NR	PLA	3-DP	CNC	20 to 1000 nm	2139		0.015*	
28	NR	PLA	3-DP	CNC	20 to 1000 nm	3534		0.025*	
27	NR	ABS	3-DP	CNC	20 to 1000 nm	1.0×10^5		0.616*	
74	NR	ABS	3-DP	CNC	20 to 1000 nm	2.1×10^4		0.125*	
57	NR	Nylon	3-DP	CNC	20 to 1000 nm	3.8×10^4		0.243*	
34	NR	PC	3-DP	CNC	20 to 1000 nm	1.7×10^5		1.143*	
180	2	PLA	3-DP	EDB/miniDiSC	7 to 400 nm	1700			H
				Resp. (PVC)	D_{50} = 5 µm			0.7	
				Inhal. (CN)	D_{50} = 100 µm			4.7	
30	NR	PLA	3-DP	EDB/miniDiSC	7 to 400 nm	3200			
				Resp. (PVC)	D_{50} = 5 µm			1.6	
				Inhal. (CN)	D_{50} = 100 µm			5.3	
40	0.22	PLA	3-DP T_n = 220 to 240	CNC	4 to 1000 nm	0.5×10^4–4.9×10^4 (P)	6.8×10^9–1.0×10^{11}		I
40	0.22	PLA Wood-1	3-DP T_n = 220 to 240	CNC	4 to 1000 nm	1.5×10^4–9.3×10^4 (P)	0.6×10^{11}–2.6×10^{11}		
40	0.22	PLA Wood-2	3-DP T_n = 230 to 240	CNC	4 to 1000 nm	7.0×10^5–9.5×10^5 (P)	1.9×10^{12}–2.8×10^{12}		
40	0.22	PLA Copper	3-DP T_n = 220 to 240	CNC	4 to 1000 nm	3.6×10^5–6.7×10^5 (P)	1.4×10^{12}–2.0×10^{12}		
40	0.22	PLA Bamboo	3-DP T_n = 210 to 240	CNC	4 to 1000 nm	0.3×10^5–9.5×10^5 (P)	1.7×10^{10}–2.7×10^{12}		
40	0.22	Flex PLA	3-DP T_n = 240	CNC	4 to 1000 nm	2.4×10^4 (P)	4.2×10^{10}		

(*Continued*)

Table 2. (Continued).

Room (m^3)	ACH (h^{-1})	Feedstock[a]	Scenario[b]	Sampler[c]	Specifics[d]	$\bar{X}C_{num}$	ER_{num}	$\bar{X}C_{mass}$	Cit.[f]
40	0.22	CP	3-DP T_n = 220 to 240	CNC	4 to 1000 nm	0.9 x 10^5–5.6 × 10^5 (P)	0.2 x 10^{12}–1.6 x 10^{12}		
40	0.22	CP-CF	3-DP T_n = 220 to 240	CNC	4 to 1000 nm	1.1 x 10^5–4.8 × 10^5 (P)	0.2 x 10^{12}–1.2 x 10^{12}		
40	0.22	Nylon	3-DP T_n = 230 to 240	CNC	4 to 1000 nm	1.3 x 10^4–1.4 × 10^4 (P)	1.4 x 10^{11}–1.6 x 10^{11}		
40	0.22	Ninja Flex®	3-DP T_n = 230 to 240	CNC	4 to 1000 nm	1.8 x 10^4–5.8 × 10^4 (P)	0.7 x 10^{11}–1.4 x 10^{11}		
33	0.3	ABS	3-DP Cover on	SMPS	10 to 420 nm	5.0 x 10^4 (P)			J
			3-DP Cover off	SMPS	10 to 420 nm	1.9 x 10^5 (P)			
NR	NR	PLA	3-DP (n = 3)	CNC	20 to 1000 nm	3.9 x 10^4			K
			3-DP (n = 4)	CNC	20 to 1000 nm	5.3 x 10^4			
			3-DP (n = 5)	CNC	20 to 1000 nm	8.7 x 10^4			
NR	NR	ABS	3-DP	SMPS	10 to 420 nm	≈ 4.0 × 10^5 (P)			L
81	5	PLA	3-DP T_n = 200	CNC	10 to 1000 nm	740	6.0 x 10^8		M
			3-DP T_n = 230	SMPS	Varied‡	3.7 x 10^5	3.1 x 10^{11}		
81	5	ABS	3-DP T_n = 230 to 238	SMPS	Varied‡	0.03–2.8 × 10^6	2.2 x 10^{10}–2.3 x 10^{12}		
			3-DP T_n = 250	SMPS	Varied‡	1.5 x 10^6	1.3 x 10^{12}		
			3-DP Malfunction	SMPS	Varied‡	4.4 x 10^5	3.7 x 10^{11}		
600	20	PLA	3-DP	CNC	10 to 1000 nm	3000			N
162	1.8	ABS	3-DP	SMPS	2 to 300 nm	3780		0.001*	
777	NR	ABS	3-DP	CNC	15 to 1000 nm	3900 (P)			O
36	NR	ABS	3-DP	SMPS	10 to 420 nm		10^3–10^5		
141	NR	ABS	3-DP	CNC	15 to 1000 nm	6.6 x 10^4 (P)			
66	NR	ABS, PC, Ultem®	FDM™ Opening doors	CNC	7 to 1000 nm	600–800			P
40	NR	ABS, PLA	3-DP Cover off	CNC	7 to 1000 nm	0.5–2.0 x 10^5			
NR	NR	ABS	3-DP Inside machine	SMPS	16 to 583 nm	6.8 x 10^5 (P)	1.1 x 10^9		Q
NR	NR	ASA	3-DP Inside machine	SMPS	16 to 583 nm	1.2 x 10^6 (P)	5.9 x 10^9		
NR	NR	PLA/PU Support	3-DP Inside machine	SMPS	16 to 583 nm	2.0 x 10^4 (P)	7.2 x 10^6		
NR	NR	CP	3-DP Inside machine	SMPS	16 to 583 nm	7.9 x 10^5 (P)	3.3 x 10^8		
NR	NR	Nylon	3-DP Inside machine	SMPS	16 to 583 nm	2.1 x 10^6 (P)	3.5 x 10^9		
NR	NR	PC	3-DP Inside machine	SMPS	16 to 583 nm	1.1 x 10^6 (P)	1.8 x 10^9		
NR	NR	PLA Green	3-DP Inside machine	SMPS	16 to 583 nm	2.5 x 10^3 (P)	1.1 x 10^6		

(*Continued*)

Table 2. (Continued).

Room (m^3)	ACH (h^{-1})	Feedstock[a]	Scenario[b]	Sampler[c]	Specifics[d]	$\bar{X}C_{num}$	ER_{num}	$\bar{X}C_{mass}$	Cit.[f]
NR	NR	PLA	3-DP	SMPS	16 to 583 nm	1.3 x 10^3 (P)	8.2 x 10^6		
		True green	Inside machine						
NR	NR	PLA	3-DP	SMPS	16 to 583 nm	1.8 x 10^3 (P)	3.8 x 10^6		
		Silver	Inside machine						
NR	NR	PLA	3-DP	SMPS	16 to 583 nm	5.6 x 10^3 (P)	1.5 x 10^6		
		PolyWood™	Inside machine						
NR	NR	PVA	3-DP	SMPS	16 to 583 nm	1.2 x 10^4	3.3 x 10^6		
			Inside machine						
NR	NR	TPU	3-DP	SMPS	16 to 583 nm	4.0 x 10^3	8.4 x 10^6		
			Inside machine						
66	NR	ABS, PC	FDM™	CNC	10 to 1000 nm		2.2 x 10^{11}		R
				OPS	0.3 to 20 µm		2.7 x 10^5		
66	NR	Ultem®	FDM™	CNC	10 to 1000 nm		4.1 x 10^{10}		
				OPS	0.3 to 20 µm		9.6 x 10^4		
40	NR	ABS, PLA	3-DP (n = 7)	CNC	20 to 1000 nm		9.7 x 10^{10}		S
76	NR	ABS	3-DP	CNC	20 to 1000 nm		7.3 x 10^{10}		
466	2	PLA	Sheer 3-DP	CNC	20 to 1000 nm		1.9 x 10^9–3.8 x 10^9		
			Sheer 3-DP	CNC	20 to 1000 nm		2.1 x 10^{11}		
			Malfunction						
			Sheer 3-DP	OPS	0.3 to 20 µm		1.0 x 10^5		
			Sheer 3-DP	OPS	0.3 to 20 µm		1.0 x 10^5		
			Malfunction						
			Sheer 3-DP	FMPS	6 to 560 nm		3.0 x 10^{11}		
			Sheer 3-DP	FMPS	6 to 560 nm		7.4 x 10^{10}		
			Malfunction						
320	NR	PLA	3-DP	CNC	20 to 1000 nm		0.6 x 10^{10}–9.0 x 10^{10}		
45	NR	PLA	3-DP	CNC	20 to 1000 nm		1.7 x 10^{11}–4.4 x 10^{11}		
195	NR	PLA	3-DP	CNC	20 to 1000 nm	6520			T
		Wood							
			3D-P	CNC	20 to 1000 nm	4.2 x 10^5			
			Malfunction						
			3D-P	LSP	0.1 to 15 µm			10	
195	NR	PLA-CF	3D-P	CNC	20 to 1000 nm	2070			
				LSP	0.1 to 15 µm			10	
195	NR	ABS-FR	3D-P	CNC	20 to 1000 nm	8.2 x 10^4			
				LSP	0.1 to 15 µm			10	
NR	1.8	ABS	3-DP	CNC	10 to 1000 nm	7.1 x 10^4			U
			Inside machine						
				SMPS	2 to 300 nm			7.6*	
14	NR	PLA	3D-P (n = 1)	CFC (PVC)	TSP			300	V
			3D-P (n = 3)	CFC (PVC)	TSP			700	
			3D-P (n = 1)	Cyclone (PVC)	D_{50} = 4 µm			800	
			3D-P (n = 3)	Cyclone (PVC)	D_{50} = 4 µm			400	
			3D-P (n = 1)	SMPS	10 to 420 nm	2303–9806			
			3D-P (n = 3)	SMPS	10 to 420 nm	9866			
						2.2 x 10^4 (P)			
303	29	PEEK	3D-P	SMPS	10 to 420 nm	≈ 1.5 × 10^5 (P)			W
			Cutting part						
153	NR	PLA	3D-P (n = 20)	SMPS	10 to 420 nm	4366–6606			X
			No LEV						

(*Continued*)

Table 2. (Continued).

Room (m^3)	ACH (h^{-1})	Feedstock[a]	Scenario[b]	Sampler[c]	Specifics[d]	$\bar{X}C_{num}$	ER_{num}	$\bar{X}C_{mass}$	Cit.[f]
46	1.9	ABS	3D-P (n = 2)[†] No HEPA filter	AMS	30 to 1000 nm			219	Y
				SMPS	15 to 685 nm		4.8×10^{10}		
46	4.0	ABS	3D-P (n = 3)[†] No HEPA filter	AMS	30 to 1000 nm			56	
				SMPS	15 to 685 nm		1.4×10^{10}		
46	3.2	PLA	3D-P (n = 3)[†] No HEPA filter	AMS	30 to 1000 nm			40	
				SMPS	15 to 685 nm		1.2×10^{9}		
355	6.3	ABS	3D-P	CNC	20 to 1000 nm	1.2×10^{4}	2.8×10^{10}		Z
65	NR	nHA	3-DP Room	miniDiSC	7 to 400	495			GG
			3-DP Room	miniDiSC	7 to 400	404			
Material jetting AM process category									
NR	NR	VeroWhite Plus RGD835	Inside machine	LSP	PM_1			30	AA
			Room air	LSP	$PM_{2.5}$			70	
				LSP	PM_{10}			3	
48	NR	VisiJet M2R-CL	Room air	LSP	Inhalable			10	T
90	0.22 estimated	TangoBlack+, VeroClear	Lid open	CNC	20 to 1000 nm		2.3×10^{10}		R
				OPS	0.3 to 20 µm				
							(1) $\times 10^{5}$		
466	2	TangoBlack+, VeroClear, VeroWhite+	Lid closed	CNC	20 to 1000 nm		1.5×10^{9}–5.5×10^{9}		
				OPS	0.3 to 20 µm		0.9×10^{4}–1.1×10^{4}		
				FMPS	5.6 to 560 nm		0.2×10^{12}–2.1×10^{12}		
Powder bed fusion AM process category									
NR	NR	Inconel 939	Cleaning	DC	10 to 300 nm	≈ 1.6×10^{4} (P)			BB
			Pre-/post-printing tasks	OPS	0.3 to 10 µm	≈ 5–30 (P)		0.5×10^{4}–4.0×10^{4} (P)	
			Near printer 1	CFC (MCE)	Cr			50	
				CFC (MCE)	Co			42	
				CFC (MCE)	Ni			110	
				CFC (MCE)	Mn			0.19	
			Near strainer 1	CFC (MCE)	Co			20	
				CFC (MCE)	Ni			53	
				CFC (MCE)	Mn			0.22	
			Near printer 2	CFC (MCE)	Cr			21	
				CFC (MCE)	Co			13	
				CFC (MCE)	Ni			48	
				CFC (MCE)	Mn			0.16	
				CFC (MCE)	Mo			2.9	
			Near strainer 2	CFC (MCE)	Cr			32	
				CFC (MCE)	Co			21	
				CFC (MCE)	Ni			71	
				CFC (MCE)	Mn			0.18	

(*Continued*)

Table 2. (Continued).

Room (m^3)	ACH (h^{-1})	Feedstock[a]	Scenario[b]	Sampler[c]	Specifics[d]	$\bar{X}C_{num}$	ER_{num}	$\bar{X}C_{mass}$	Cit.[f]
				CFC (MCE)	Mo			3.2	
1176	NR	Nylon-12 Glass filler	Printing	CNC	< 1000 nm	1.7×10^4			T
				LSP	0.1 to 15 µm			40	
			Post-printing/processing	LSP	0.1 to 15 µm			400	
991	NR	Nylon-12 Glass filler	MJF printing	CNC	< 1000 nm	1110			
				LSP	0.1 to 15 µm			50	
			Post-printing/processing	LSP	0.1 to 15 µm			190	
117	NR	Nylon-12	Pre-printing Virgin powder	LSP	0.1 to 15 µm			523	CC
			Pre-printing Recyc. powder	LSP	0.1 to 15 µm			706	
			Printing Virgin powder	LSP	0.1 to 15 µm			39	
			Printing Recyc. powder	LSP	0.1 to 15 µm			46	
			Post-printing Virgin powder	LSP	0.1 to 15 µm			46	
			Post-printing Recyc. powder	LSP	0.1 to 15 µm			95	
NR	NR	316 L SS	Oper. station Day 1	NSAM	10 to 487 nm	457			DD
			Oper. station Day 2	NSAM	10 to 487 nm	294			
			Oper. station Day 3	NSAM	10 to 487 nm	379			
			Oper. station Day 1	SMPS	10 to 420 nm	1.8×10^4			
			Oper. station Day 2	SMPS	10 to 420 nm	1.2×10^4			
			Oper. station Day 3	SMPS	10 to 420 nm	1.5×10^4			
			Machine rear Day 1	SMPS	10 to 420 nm	6021			
			Machine rear Day 2	SMPS	10 to 420 nm	5262			
			Machine rear Day 3	SMPS	10 to 420 nm	6384			
			Feeding silos Day 1	SMPS	10 to 420 nm	6382			
			Feeding silos Day 2	SMPS	10 to 420 nm	5610			
			Feeding silos Day 3	SMPS	10 to 420 nm	6774			
NR	NR	304 L SS	NR	DC	10 to 300 nm	6300			EE
148	9.3	Nylon-12	Printing	CNC	20 to 1000 nm	1.5×10^4	2.8×10^{10}		Z
			Phase I	LSP	0.1 to 15 µm			110–450	
			Phase II	LSP	0.1 to 15 µm			510–1790	
			Pouring	LSP	0.1 to 15 µm			1.5×10^5	
NR	NR	Ti6Al4V	Emptying @ FF	CNC	10 to 1000 nm	1.5×10^3			FF
			Opening PRS, Cleaning @ FF	CNC	10 to 1000 nm	2.5×10^3			
			Grinding @ FF	CNC	10 to 1000 nm	1.5×10^4			
			Grinding @ NF	CNC	10 to 1000 nm	2.5×10^5			

(*Continued*)

Table 2. (Continued).

Room (m^3)	ACH (h^{-1})	Feedstock[a]	Scenario[b]	Sampler[c]	Specifics[d]	$\bar{X}C_{num}$	ER_{num}	$\bar{X}C_{mass}$	Cit.[f]
			Printing @ NF	LSP	Respirable			58.4	
			Printing @ NF	Cyclone (TF)	Respirable			50.4	
Vat photopolymerization AM process category									
55	NR	VarseoWax	Scenario 1 Outside machine <1 m (printing)	CNC	20 to 1000 nm	8020			T
				LSP	Inhalable			50	

[a]ABS = acrylonitrile butadiene styrene, ASA = acrylonitrile styrene acrylate, CF = carbon fiber additive, CP = co-polyester, FR = flame retardant additive, nHA = nanoscale hydroxyapatite in unspecified polymer matrix, PC = polycarbonate, PEEK = poly ether ether ketone, PLA = polylactic acid, PU = polyurethane, PVA = polyvinyl alcohol, SS = stainless steel, TPU = thermoplastic polyurethane

[b]3-DP = desktop-scale fused filament fabrication 3D printer, FDM™ = industrial-scale fused deposition modeling machine, FF = far-field, HEPA = high-efficiency particulate air filter, LEV = local exhaust ventilation, MJF = multi-jet fusion machine, NF = near-field, PRS = powder removal system, R_f = filament feed rate (mm/s), T_n = extruder nozzle temperature (°C)

[c]AMS = aerosol mass spectrometer, CFC = close-faced cassette, CN = cellulose nitrate filter, CNC = condensation nuclei counter, DC = diffusion charger, EDB = electrometer-based diffusion battery, FMPS = fast mobility particle sizer, Respirable = respirable sampler (e.g., FSP-10 cyclone or GK2.69 cyclone), Inhal. = inhalable sampler (e.g., Button, GSP-10, or Institute of Occupational Medicine [IOM] sampler), LSP = light scattering photometer (e.g., DustTrak™ or environmental particulate air monitor), NSAM = nanoparticle surface area monitor, MCE = mixed cellulose ester filter, OPS = optical particle sizer, PVC = polyvinyl chloride filter, Resp. = respirable sampler (e.g., nylon, aluminum, or FSP10 cyclone), SMPS = scanning mobility particle sizer, TF = Teflon® (polytetrafluoroethylene) filter

[d]Co = cobalt, Cr = chromium, D_{50} = 50% aerodynamic particle diameter cutoff, Fe = iron, Mn = manganese, Mo = molybdenum, Ni = nickel, PM_x = particulate matter with aerodynamic diameter less than 1 µm, 2.5 µm, or 10 µm, PNOC = particulate not otherwise classified, TSP = total suspended particulate

[e]*P* = peak

[f]A = Afshar-Mohajer et al. (2015), B = Lewinski, Secondo, and Ferri (2019), C = Bau et al. (2020), D = Stephens et al. (2013), E = Zhou et al. (2015), F = Deng et al. (2016), G = McDonnell et al. (2016), H = Steinle (2016), I = Stabile et al. (2017), J = Yi et al. (2016), K = Bharti and Singh (2017), L = Simon, Aguilera, and Zhao (2017), M = Mendes et al. (2017), N = Zontek et al. (2017), O = Vance et al. (2017), *P* = Du Preez et al. (2018b), Q = Chýlek et al. (2019), R = Stefaniak, Johnson, du Preez, Hammond, Wells, Ham, LeBouf, Martin, et al. (2019b), S = Stefaniak, Johnson, du Preez, Hammond, Wells, Ham, LeBouf, Menchaca, et al. (2019c), T = Väisänen et al. (2019), U = Zontek et al. (2019), V = Chan et al. (2020), W = Dunn, Dunn, et al. (2020a), X = Dunn, Hammond, et al. (2020b), Y = Katz et al. (2020), Z = Zisook et al. (2020), AA = Ryan and Hubbard (2016), BB = Graff et al. (2017), CC = Damanhuri, Subki, et al. (2019b), DD = Gomes et al. (2019), EE = Ljunggren et al. (2019), FF = Jensen et al. (2020), GG = Oberbek et al. (2019)

* Calculated by study authors assuming spherical particle shape and density of polymer

‡Authors report using one brand of SMPS at different inlet flows corresponding to size ranges of 2 to 65 nm and 4.5 to 141 nm and another brand of SMPS with size range 5.5 to 350 nm, but report results as "SMPS"

†50^{th} percentile value reported for all printers in a scenario was divided by number of printers in use to obtain unit specific emission rates

NR = not reported

Directed energy deposition

Only one study has reported emissions from a DED process in a manufacturing facility (room volume and ACH not reported). In that study, during printing, particle number concentration measured using a condensation nuclei counter (CNC) was 0.5×10^6 to 1.5×10^6 #/cm^3. Personal breathing zone (PBZ) monitoring was performed for metals, though no samples were collected for organic chemicals.

Bau et al. characterized airborne particle emissions and assessed operator's exposure to airborne particles during DED utilizing 316 L stainless steel and Inconel 625 powder feedstocks (Bau et al. 2020). The operating procedure composed of 20-minute production cycles to evaluate the two materials while using two injection nozzles. Sampling took place at three locations during the manufacturing process and the transient door opening phase; simultaneously, the operator's personal exposure to hexavalent chromium [Cr(VI)] was assessed. Emitted particles were often only a few nanometers in diameter and more than 90% were smaller than 250 nm. From Table 2, their compositions corresponded with the feedstock powder, i.e., were predominantly iron (Fe), chromium (Cr), manganese (Mn), molybdenum (Mo), and nickel (Ni); traces of Cr(VI) were quantified on some area samples. The operator's exposure to Cr(VI) was below the analytical method limit of quantitation (LOQ) of 98 μg/m^3 for both feedstock powders. Personal exposure monitoring using a DiSCmini sampler worn by the operator indicated an increase in particle number concentration after the completion of each production cycle (5.0 x 10^6 #/cm^3). During the production cycles, near field number and mass concentrations were ~10^4 #/cm^3 and below 40 μg/m^3, although far-field number concentrations were also on the order of 10^4 #/cm^3. Results from the transient door opening task indicated high levels of particles (i.e., > 10^5 #/cm^3) similar with near field results. High levels of particles (> 5×10^5 #/cm^3, 300 to 1300 μg/m^3 inhalable particles, and 200 to 6000 μg Cr(VI)/m^3) were released inside the machine enclosure during the different production cycles. Both the material type and injection nozzle (10VX and 24VX) had a significant effect on particle number concentration. The 316 L stainless steel had the lowest particle number concentrations when the 24 VX nozzle was used, while Inconel 625 had the highest particle number concentrations with the 10VX nozzle. There are no apparent data on emissions from DED using wire feedstock; however, electric arc DED is similar to robotic electric arc welding and relevant literature was recently reviewed to describe AM worker health risks (Nagarajan et al. 2020).

Material extrusion

Twenty-eight publications contributed knowledge to current understanding of emission characteristics, factors that influence emissions, and factors that influence exposures for the ME process category. These publications reported measurements of ME processes at 39 different sites (Table 3), which included university labs, offices, school classrooms, college dormitories, research and development facilities, and manufacturing workplaces. Room characteristics ranged from an 8 m^3 clean room (0.1 ACH) to a 777 m^3 office workspace (ACH not reported). Among all investigations, particle ERs ranged from 1×10^5 #/min to 2.8×10^{12} #/min, which reflected differences in feedstock materials, printer design, printing parameters, room characteristics, and sampling instrumentation. From these assessments, average TVOC concentrations ranged from 0.7 μg/m^3 to 9×10^5 μg/m^3 and reported TVOC ERs were 2 to 3300 mg/min (Table 4). Personal exposure monitoring was performed for metals and organic gases, though all levels were below appropriate OELs.

Emission characteristics

Stephens et al. (2013) evaluated emissions from up to five desktop-scale FFF 3D printers while extruding ABS and PLA filaments using an SMPS and all particle counts had sizes that were smaller than 150 nm. Zhou et al. (2015) used an OPS to assess emissions from desktop-scale FFF 3D printers during extrusion of ABS filament. The highest number concentration was in the smallest size bin of the instrument, 250 to 280 nm, with almost no counts above 375 nm (Zhou et al. 2015). Multiple investigators have since demonstrated that particles emitted during desktop-scale FFF 3D printing were predominantly in the ultrafine (d < 100 nm) size range (Chan et al. 2020; Chýlek et al. 2019; Ding, Wan, and Ng 2020; Dunn et al. 2020a; Katz

Table 3. Summary of particle-phase personal breathing zone exposures among additive manufacturing workers.

Room (m^3)	ACH (h^{-1})	Feedstock[a]	Scenario[b]	Sampler[c]	Specifics	Analysis[d]	Analyte[e]	C ($\mu g/m^3$)	Cit.[f]
Directed energy deposition AM process category									
NR	NR	316 L SS	End of build	miniDiSC	Real-time	n/a	Particles	5.0 x 10^6 #	A
Material extrusion AM process category									
66	NR	ABS, PLA Employee 1	3-DP	NRD	10 to 300 nm	ICP-MS	Al	10	B
40	NR	ABS, PLA Employee 1	3-DP/AVP	NRD	10 to 300 nm	ICP-MS	Al	20	
40	NR	ABS, PLA Employee 2	3-DP/AVP	NRD	10 to 300 nm	ICP-MS	Fe	10	
66	NR	ABS, PC	FDM™	NRD	10 to 300 nm	ICP-MS	Al	Up to 10	C
				NRD	10 to 300 nm	ICP-MS	Fe	Up to 10	
40	NR	ABS, PLA	3-DP	NRD	10 to 300 nm	ICP-MS	Al	10–20	D
76	NR	ABS	3-DP	NRD	10 to 300 nm	ICP-MS	Al	10–20	
303	29	PEEK CNF/CNT	3-DP	OFC (MCE)	Total	TEM	CNF/CNT	Present*	E
Material jetting AM process category									
90	0.22 estimated	TangoBlack+, VeroClear	Printing	NRD	10 to 300 nm	ICP-MS	Al	Up to 10	C
				NRD	10 to 300 nm	ICP-MS	Fe	Up to 10	
Powder bed fusion AM process category									
NR	NR	Inconel 939	Pre-/printing tasks	CFC (MCE)	Total	ICP-MS	Cr	44	F
				CFC (MCE)	Total	ICP-MS	Co	38	
				CFC (MCE)	Total	ICP-MS	Ni	99	
				CFC (MCE)	Total	ICP-MS	Mn	0.17	
NR	NR	Inconel 718, Ti64	Pre-/post-printing tasks	Cyclone (CN)	Inhalable	GF-AAS	Ni	12.5	G
				Cyclone (CN)	Inhalable	GF-AAS	Cr	3.5	
				Cyclone (CN)	Inhalable	ICP-MS	Fe	10	
				Cyclone (CN)	Inhalable	GF-AAS	Ti	11.5	
				Cyclone (CN)	Inhalable	FAAS	Al	104	
				Cyclone (CN)	Respirable	GF-AAS	Ni	0.6	
				Cyclone (CN)	Respirable	GF-AAS	Ti	1.6	
NR	NR	304 L SS	Printing – Year 1	IOM (MCE)	Inhalable	ICP-MS	Cr	6.8–86.8	H
				IOM (MCE)	Inhalable	ICP-MS	Fe	114.7–253.8	
				IOM (MCE)	Inhalable	ICP-MS	Ni	6.6–268.9	
			Printing – Year 2	IOM (MCE)	Inhalable	ICP-MS	Cr	3.0–331.0	
				IOM (MCE)	Inhalable	ICP-MS	Fe	23.9–283.3	
				IOM (MCE)	Inhalable	ICP-MS	Ni	5.1–715.7	
			Printing – Year 1	OFC (MCE)	Total dust	ICP-MS	Cr	2.0–59.4	
				OFC (MCE)	Total dust	ICP-MS	Fe	100.8–253.8	
				OFC (MCE)	Total dust	ICP-MS	Ni	2.0–256.1	
NR	NR	Ti6Al4V	Emptying print chamber	miniDiSC	Real-time	n/a	Particles	4.2 x10^3	I
			PRS closed	miniDiSC	Real-time	n/a	Particles	0.6 x10^3	
			PRS open	miniDiSC	Real-time	n/a	Particles	1.5 x10^3	
			Baking	miniDiSC	Real-time	n/a	Particles	1.0 x10^3	
			Grinding	miniDiSC	Real-time	n/a	Particles	3.6 x10^4	

[a]ABS = acrylonitrile butadiene styrene, CNF = carbon nanofiber, CNT = carbon nanotube, PC = polycarbonate, PEEK = poly ether ether ketone, PLA = polylactic acid, SS = stainless steel

[b]3-DP = desktop-scale fused filament fabrication 3-D printer, AVP = acetone vapor polishing post-processing task, FDM™ = industrial-scale fused deposition modeling machine, PRS = powder removal system

[c]CFC = close-faced cassette, CN = cellulose nitrate filter, MCE = mixed cellulose ester filter, OFC = open-faced cassette, NRD = nanoparticle respiratory deposition sampler

[d]FAAS = flame atomic absorption spectrometry, GF-AAS = graphite furnace-atomic absorption spectrometry, ICP-MS = inductively coupled plasma-mass spectrometry, TEM = transmission electron microscopy

[e]Al = aluminum, CNF = carbon nanofiber, CNT = carbon nanotube, Co = cobalt, Cr = chromium, Fe = iron, Mn = manganese, Ni = nickel, Ti = titanium

[f]A = Bau et al. (2020), B = Du Preez et al. (2018b), C = Stefaniak, Johnson, du Preez, Hammond, Wells, Ham, LeBouf, Martin, et al. (2019b), D = Stefaniak, Johnson, du Preez, Hammond, Wells, Ham, LeBouf, Menchaca, et al. (2019c), E = Dunn, Dunn, et al. (2020), F = Graff et al. (2017), G = Walter et al. (2018), H = Ljunggren et al. (2019), I = Jensen et al. (2020)

= number concentration (#/cm^3)

* Free CNT and polymer particles that contained CNF/CNT

NR = not reported

Table 4. Summary of gas-phase releases (emission rates and concentrations) from additive manufacturing machines by process type.

Room (m^3)	ACH (h^{-1})	Feedstock[a]	Scenario[b]	Sampler[c]	Specifics[d]	Analysis[e]	Analyte[f]	$\bar{X}C$ (µg/m^3)[g]	ER (mg/min)	Cit.[h]
Binder jetting AM process category										
157	6	Gypsum	Cover shut	PID	10.6 eV	n/a	TVOC	1725 (P)	22–27	A
Material extrusion AM process category										
28	NR	PLA	3-DP	PID	10.6 eV	n/a	TVOC	102 480 (P)		B
544	NR	PLA	3-DP	PID	10.6 eV	n/a	TVOC	408 734 (P)		
28	NR	PLA	3-DP	PID	10.6 eV	n/a	TVOC	578 1010 (P)		
27	NR	ABS	3-DP	PID	10.6 eV	n/a	TVOC	186 333 (P)		
74	NR	ABS	3-DP	PID	10.6 eV	n/a	TVOC	172 365 (P)		
57	NR	Nylon	3-DP	PID	10.6 eV	n/a	TVOC	2570 3534 (P)		
34	NR	PC	3-DP	PID	10.6 eV	n/a	TVOC	895 6504 (P)		
180	2	PLA	3-DP	PID	10.6 eV	n/a	TVOC	33–38		C
				TD Tube	Tenax®	GC-MS	MM	0.7		
30	NR	PLA	3-DP	PID	10.6 eV	n/a	TVOC	92–216		
			3-DP	TD Tube	Tenax®	GC-MS	MM	5.5–19		
81	5	ABS, PLA	3-DP	Cartridge	Silica gel	LC-MS	Formaldehyde	2–3		D
40	NR	ABS	AVP	TD tube	SVI	GC-MS	Acetone	100		E
				PID	10.6 eV	n/a	TVOC	9.0×10^5		
40	NR	PLA	CVP Pouring $CHCl_3$	PID	10.6 eV	n/a	TVOC	2.4×10^5		
			CVP Brushing $CHCl_3$	PID	10.6 eV	n/a	TVOC	1.0×10^5–2.0×10^5		
66	NR	ABS, PC	FDM™	PID	10.6 eV	n/a	TVOC		19	F
				Gas sensor	SC	n/a	Ozone	37		
66	NR	ABS, PC Morning	FDM™	TD tube	SVI	GC-MS	Acetone	0.6×10^4–3.3×10^4		
66	NR	ABS, PC Afternoon	FDM™	TD tube	SVI	GC-MS	Acetone	0.3×10^4–1.6×10^4		
66	NR	Ultem®	FDM™	PID	10.6 eV	n/a	TVOC		94	
				Gas sensor	SC	n/a	Ozone	43		
				TD tube	SVI	GC-MS	Acetone	400		
40	NR	ABS, PLA	3-DP (n = 7)	PID	10.6 eV	n/a	TVOC		3300	G
				TD tube	SVI	GC-MS	Acetone	98.7		
				TD tube	SVI	GC-MS	IPA	122.2		
76	NR	ABS	3-DP	PID	10.6 eV	n/a	TVOC		120	

(*Continued*)

Table 4. (Continued).

Room (m^3)	ACH (h^{-1})	Feedstock[a]	Scenario[b]	Sampler[c]	Specifics[d]	Analysis[e]	Analyte[f]	$\bar{X}C$ ($\mu g/m^3$)[g]	ER (mg/min)	Cit.[h]
				TD tube	SVI	GC-MS	Acetone	457		
				TD tube	SVI	GC-MS	Benzene	8.2		
				TD tube	SVI	GC-MS	Hexane	7.7		
				TD tube	SVI	GC-MS	IPA	4637		
466	2	PLA	Sheer 3-DP	PID	10.6 eV	n/a	TVOC		16–31	
			Sheer 3-DP Malfunction	PID	10.6 eV	n/a	TVOC		23	
320	NR	PLA	3-DP	PID	10.6 eV	n/a	TVOC		2–44	
45	NR	PLA	3-DP	PID	10.6 eV	n/a	TVOC		8–11	
				TD tube	SVI	GC-MS	Acetaldehyde	43.0–43.1		
				TD tube	SVI	GC-MS	Acetone	222–273		
				TD tube	SVI	GC-MS	IPA	2.3×10^4–4.1×10^4		
				TD tube	SVI	GC-MS	MC	6.3–9.2		
195	NR	PLA EasyWood™	3-DP	TD Tube	Tenax® TA	GC-MS	Decanal	8		H
				TD Tube	Tenax® TA	GC-MS	DCPS	8		
				TD Tube	Tenax® TA	GC-MS	BEA	16		
				TD Tube	Tenax® TA	GC-MS	PG	17		
				TD Tube	Tenax® TA	GC-MS	TVOC (ΣVOC_i)	117		
				Sorbent tube	DNPH	HPLC-UV	Formaldehyde	11		
				Sorbent tube	DNPH	HPLC-UV	Acetone	17		
				Sorbent tube	DNPH	HPLC-UV	Butanone	15		
195	NR	PLA-CF	3-DP	TD Tube	Tenax® TA	GC-MS	DCPS	11		
				TD Tube	Tenax® TA	GC-MS	Decanal	15		
				TD Tube	Tenax® TA	GC-MS	BEA	44		
				TD Tube	Tenax® TA	GC-MS	Benzoic acid	47		
				TD Tube	Tenax® TA	GC-MS	TVOC (ΣVOC_i)	180		
				Sorbent tube	DNPH	HPLC-UV	Formaldehyde	14		
				Sorbent tube	DNPH	HPLC-UV	Acetone	20		
				Sorbent tube	DNPH	HPLC-UV	Butanone	14		
195	NR	ABS-FR	3-DP	TD Tube	Tenax® TA	GC-MS	Decanal	23		
				TD Tube	Tenax® TA	GC-MS	NDEE	23		
				TD Tube	Tenax® TA	GC-MS	BEA	26		
				TD Tube	Tenax® TA	GC-MS	I. Myristate	34		
				TD Tube	Tenax® TA	GC-MS	TVOC (ΣVOC_i)	338		
195	NR	ABS-FR	3-DP	Sorbent tube	DNPH	HPLC-UV	Formaldehyde	18		
				Sorbent tube	DNPH	HPLC-UV	Acetaldehyde	8		
				Sorbent tube	DNPH	HPLC-UV	Acetone	74		
				Sorbent tube	DNPH	HPLC-UV	Butanone	8		

(*Continued*)

Table 4. (Continued).

Room (m^3)	ACH (h^{-1})	Feedstock[a]	Scenario[b]	Sampler[c]	Specifics[d]	Analysis[e]	Analyte[f]	$\bar{X}C$ ($\mu g/m^3$)[g]	ER (mg/min)	Cit.[h]
NR	NR	ABS	3-DP Inside machine	Sorbent tube	Charcoal	GC-MS	Toluene	16		I
				Sorbent tube	Charcoal	GC-MS	Styrene	69		
				Sorbent tube	Charcoal	GC-MS	TVOC	391		
NR	NR	PLA	3-DP Inside machine	Sorbent tube	Charcoal	GC-MS	Toluene	26		
				Sorbent tube	Charcoal	GC-MS	Styrene	21		
				Sorbent tube	Charcoal	GC-MS	TVOC	255		
NR	NR	PET	3-DP Inside machine	Sorbent tube	Charcoal	GC-MS	Toluene	11		
				Sorbent tube	Charcoal	GC-MS	Styrene	6		
				Sorbent tube	Charcoal	GC-MS	TVOC	151		
126	NR	PLA	3-DP (n = 5)	TD Tube	Tenax® TA	GC-MS	Acrylonitrile	7.3		J
				TD Tube	Tenax® TA	GC-MS	MC	5.7		
				TD Tube	Tenax® TA	GC-MS	Hexane	29.8		
				TD Tube	Tenax® TA	GC-MS	Toluene	6.2		
				TD Tube	Tenax® TA	GC-MS	Xylenes	5.6		
14	NR	PLA	3-DP (n = 1)	Sorbent tube	DNPH	HPLC-UV	Formaldehyde	4.9		K
				TD Tube	Sorbent	GC-MS	IPA	190		
				TD Tube	Sorbent	GC-MS	Acetone	10		
				TD Tube	Sorbent	GC-MS	TVOC	270		
14	NR	PLA	3-DP (n = 3)	Sorbent tube	DNPH	HPLC-UV	Formaldehyde	4.5		
				TD Tube	Sorbent	GC-MS	IPA	1400		
				TD Tube	Sorbent	GC-MS	Acetone	110		
				TD Tube	Sorbent	GC-MS	Ethanol	77		
				TD Tube	Sorbent	GC-MS	TVOC	1700		
355	6.3	ABS	3D-P	Minican	Si-lined	GC-MS	IPA	2260		L
NR	NR	ABS	3D-P Inside machine	OE nose	Dye-based	Digital	Cyclohexanone	Present		M
							Ethylbenzene	Present		
							Isobutanol	Present		
							Styrene	Present		
		PLA	3D-P Inside machine	OE nose	Dye-based	Digital	Acetone			
							Isobutanol	Present		
							Lactide	Present		
							MM	Present		
		PETG	3D-P Inside machine	OE nose	Dye-based	Digital	Acetone	Present		
							Formaldehyde	Present		
							Toluene	Present		

(*Continued*)

Table 4. (Continued).

Room (m^3)	ACH (h^{-1})	Feedstock[a]	Scenario[b]	Sampler[c]	Specifics[d]	Analysis[e]	Analyte[f]	$\bar{X}$C (µg/m^3)[g]	ER (mg/min)	Cit.[h]
Material jetting AM process category										
48	NR	VisiJet M2R-CL	Printing	TD Tube	Tenax®	GC-MS	Iso. acrylate	1325–2076		H
				TD Tube	Tenax®	GC-MS	2-Furn.	127–164		
				TD Tube	Tenax®	GC-MS	BHT	61–113		
				TD Tube	Tenax®	GC-MS	*o*-Xylene	64–102		
				TD Tube	Tenax®	GC-MS	TVOC	2001–2872		
			Post-processing	TD Tube	Tenax®	GC-MS	Iso. acrylate	1233		
				TD Tube	Tenax®	GC-MS	BHT	225		
				TD Tube	Tenax®	GC-MS	2-Furan.	112		
				TD Tube	Tenax®	GC-MS	*m,p*-Xylene	76		
				TD Tube	Tenax®	GC-MS	TVOC	1809		
90	0.22 estimated	TangoBlack+, VeroClear	Lid open	PID	10.6 eV	n/a	TVOC		2.8×10^4	F
				TD tube	SVI	GC-MS	Acetaldehyde	54		
				TD tube	SVI	GC-MS	Ethanol	1.1×10^4		
				Gas sampler	SC	n/a	Ozone	26.3		
466	2	TangoBlack+, VeroClear, VeroWhite+	Lid closed	PID	10.6 eV	n/a	TVOC		2.5×10^4–4.5×10^4	
				TD tube	SVI	GC-Ms	Acetaldehyde	14–214		
				Canister	Evacuated	GC-MS	Ethanol	70.6		
				Canister	Evacuated	GC-MS	IPA	149–342		
				Canister	Evacuated	GC-MS	MM	4.4		
				Gas sensor	SC	n/a	Ozone	9–11		
Powder bed fusion AM process category										
1176	NR	Nylon-12 Glass filler	Printing	TD Tube	Tenax®	GC-MS	Siloxanes	27		H
				TD Tube	Tenax®	GC-MS	TVOC	113		
				TD Tube	Tenax®	GC-MS	Formaldehyde	40		
				TD Tube	Tenax®	GC-MS	Acetaldehyde	42		
				IAQ-Calc™	NDIR	n/a	CO_2	450 ppm		
				IAQ-Calc™	EC	n/a	CO	0.1 ppm		
991	NR	Nylon-12 Glass filler	MJF	TD Tube	Tenax®	GC-MS	Alcohols	223		
				TD Tube	Tenax®	GC-MS	Aliphatic hydrocarbons	59		
				TD Tube	Tenax®	GC-MS	Aromatic hydrocarbons	161		
				TD Tube	Tenax®	GC-MS	TVOC	1114		
				TD Tube	Tenax®	GC-MS	Acetone	41		
				IAQ-Calc™	NDIR	n/a	CO_2	680 ppm		

(*Continued*)

Table 4. (Continued).

Room (m^3)	ACH (h^{-1})	Feedstock[a]	Scenario[b]	Sampler[c]	Specifics[d]	Analysis[e]	Analyte[f]	$\bar{X}C$ ($\mu g/m^3$)[g]	ER (mg/min)	Cit.[h]
				IAQ-Calc™	EC	n/a	CO	0.4 ppm		
117	NR	Nylon-12	Pre-printing Virgin powder	PID	10.6 eV	n/a	TVOC	872		N
			Pre-printing Recyc. powder	PID	10.6 eV	n/a	TVOC	620		
			Printing Virgin powder	PID	10.6 eV	n/a	TVOC	528		
			Printing Recyc. powder	PID	10.6 eV	n/a	TVOC	1285		
			Post-printing Virgin powder	PID	10.6 eV	n/a	TVOC	803		
			Post-printing Recyc. powder	PID	10.6 eV	n/a	TVOC	2410		
		Nylon-12	Pre-printing Virgin powder	Gas sensor	NDIR	n/a	CO_2	954 ppm		
			Pre-printing Recyc. powder	Gas sensor	NDIR	n/a	CO_2	914 ppm		
			Printing Virgin powder	Gas sensor	NDIR	n/a	CO_2	613 ppm		
			Printing Recyc. powder	Gas sensor	NDIR	n/a	CO_2	577 ppm		
			Post-printing Virgin powder	Gas sensor	NDIR	n/a	CO_2	757 ppm		
			Post-printing Recyc. powder	Gas sensor	NDIR	n/a	CO_2	869 ppm		
117	NR	Nylon-12	Pre-printing	PID	10.6 eV	n/a	TVOC	872		O
			Printing	PID	10.6 eV	n/a	TVOC	544		
			Post-printing	PID	10.6 eV	n/a	TVOC	817		
			Pre-printing	Gas sensor	EC	n/a	Formaldehyde	49		
			Printing	Gas sensor	EC	n/a	Formaldehyde	32		
			Post-printing	Gas sensor	EC	n/a	Formaldehyde	45		
117	NR	Nylon-12	Printing	Canister	Evacuated	GC-MS	IPA	442		L
				Canister	Evacuated	GC-MS	Propylene	45		
Vat photopolymerization AM process category										
NR	NR	Resin	Drilling parts	Badge	Passive	GC-MS	IPA	590		P
55	NR	VarseoWax	Scenario 1 Outside machine <1 m (printing)	TD Tube	Tenax®	GC-MS	THF alcohol	18		H
				TD Tube	Tenax®	GC-MS	*p*-Xylene	13–16		
				TD Tube	Tenax®	GC-MS	MM	136		
				TD Tube	Tenax®	GC-MS	2-BAME	55–63		
				TD Tube	Tenax®	GC-MS	4-M-2-P	3–76		
				TD Tube	Tenax®	GC-MS	TVOC	182–427		
				Sorbent tube	DNPH	HPLC-UV	Formaldehyde	12		
				Sorbent tube	DNPH	HPLC-UV	Acetone	136		
				IAQ-Calc™	NDIR	n/a	CO_2	550–860 ppm		
				IAQ-Calc™	EC	n/a	CO	0–1.8 ppm		
			Part washing	TD Tube	Tenax®	GC-MS	Ethanol	139		

(*Continued*)

Table 4. (Continued).

Room (m^3)	ACH (h^{-1})	Feedstock[a]	Scenario[b]	Sampler[c]	Specifics[d]	Analysis[e]	Analyte[f]	$\bar{X}$C ($\mu g/m^3$)[g]	ER (mg/min)	Cit.[h]
				TD Tube	Tenax®	GC-MS	IPA	1658		
				TD Tube	Tenax®	GC-MS	TFP	442		
				TD Tube	Tenax®	GC-MS	MM	292		
				TD Tube	Tenax®	GC-MS	4-M-2-P	8139		
				TD Tube	Tenax®	GC-MS	TVOC	11084		
155	NR	Grey & Castable resins	Scenario 2 Outside machine <1 m (printing)	TD Tube	Tenax®	GC-MS	IPA	8–24		
				TD Tube	Tenax®	GC-MS	Acetic acid	28		
				TD Tube	Tenax®	GC-MS	MM	35–93		
				TD Tube	Tenax®	GC-MS	EM	14–34		
				TD Tube	Tenax®	GC-MS	TVOC	84–176		
				Sorbent tube	DNPH	HPLC-UV	Acetone	17		
				Sorbent tube	DNPH	HPLC-UV	Butanone	22		
				IAQ-Calc™	NDIR	n/a	CO_2	470–650 ppm		
NR	NR	White resin	Drilling models	Badge	Passive	GC-MS	IPA	590		P
28	8.6	Epoxy resin	Printing	Impinger	Liquid trap	ISE	Fluorine*	5.1		L
				Canister	Evacuated	GC-MS	Acetone	582		
							IPA	1377		
41	NR	MM resin	Printing	PID	10.6 eV	n/a	TVOC	1053		Q
			Curing and washing	PID	10.6 eV	n/a	TVOC	1774		

[a]ABS = acrylonitrile butadiene styrene, CF = carbon fiber additive, FR = flame retardant additive, MM = methyl methacrylate, PC = polycarbonate, PET = polyethylene terephthalate, PETG = PET glycol, PLA = polylactic acid

[b]3-DP = desktop-scale fused filament fabrication 3D printer, AVP = acetone vapor polishing task, CVP = chloroform ($CHCl_3$) vapor polishing task, FDM™ = industrial-scale fused deposition modeling machine, MJF = multi-jet fusion machine

[c]OE = optoelectronic nose, PID = photoionization detector, TD = thermal desorption

[d]DNPH = 2,4-Dinitrophenylhydrazine-coated silica gel sorbent, EC = electrochemical sensor, eV = electron volt, NDIR = non-dispersive infrared, SC = semiconductor sensor, SVI = soil vapor intrusion

[e]GC = gas chromatography, HPLC = high-performance liquid chromatography, ISE = ion selective electrode, LC = liquid chromatography, MS = mass spectrometry, UV = ultraviolet detector

[f]2-BAME = 2-buteinic acid methyl ester, 2-Furn. = 2-furnapropanoic acid, 4-M-2-*P* = 4-methyl-2-pentanone, BEA = 2-(2-butoxyethoxy)ethyl acetate, BHT = butylated hydroxytoluene, CO = carbon monoxide, CO_2 = carbon dioxide, DCPS = decamethylcyclopentasiloxane, EM = ethyl methacrylate, I. Myristate = isopropyl myristate, IPA = isopropyl alcohol, Iso. acrylate = isobornyl acrylate, MC = methylene chloride, MM = methyl methacrylate, NDEE = N-[3,4-dimethylphenyl]-ethyl ester, PG = propylene glycol, TFP = tetrahydro-2-furnyl methyl pivalate, THF = tetrahydrofurfyl, TVOC = total volatile organic compounds, TVOC ΣVOC_i = TVOC calculated as sum of all individual VOCs on a sample

[g]*P* = peak

[h]A = Afshar-Mohajer et al. (2015), McDonnell et al. (2016), C = Steinle (2016), D = Mendes et al. (2017), E = Du Preez et al. (2018b), F = Stefaniak, Johnson, du Preez, Hammond, Wells, Ham, LeBouf, Martin, et al. (2019b), G = Stefaniak, Johnson, du Preez, Hammond, Wells, Ham, LeBouf, Menchaca, et al. (2019c), H = Väisänen et al. (2019), I = Bravi, Murmura, and Santos (2019), J = Youn et al. (2019), K = Chan et al. (2020), L = Zisook et al. (2020), M = Pinheiro et al. (2021), N = Damanhuri, Subki, et al. (2019b), O = Damanhuri, Hariri, et al. (2019a), *P* = Freiser et al. (2018), Q = Yang and Li (2018)

NR = not reported

* total fluorine (aerosol and gas)

et al. 2020; Mendes et al. 2017; Stabile et al. 2017; Stefaniak et al. 2019c; Vance et al. 2017; Youn et al. 2019; Zontek et al. 2019, 2017). There is no clear relationship between emitted particle size and polymer type or extrusion temperature (Chýlek et al. 2019; Stabile et al. 2017).

The nanoscale size of particles released during ME processes can present challenges for characterization of the physical and chemical properties of individual particles (Mendes et al. 2017). Steinle (2016) used transmission electron microscopy (TEM) to visualize particle morphology and size with energy dispersive x-ray (EDX) analysis to identify elemental constituents of individual particles that were released from a FFF 3D printer during extrusion of PLA polymer. Two distinct morphology regimes were observed, nanoscale semi-spherical-shaped particles and nanoscale cluster particles with soot-like appearance that were composed of approximately 10 to 20 nm primary particles. Some semi-spherical particles contained potassium (K) and sulfur (S) and the cluster particles were composed of carbon. Zontek et al. (2017) employed TEM-EDX to characterize aerosol released from FFF 3D printers during extrusion of ABS and PLA polymers and observed similar particle morphology regimes as Steinle (2016); some particles contained aluminum (Al), silicon (Si), S, and/or titanium (Ti) (Zontek et al. 2017). As illustrated in Figure 4, other investigators subsequently confirmed the release of soot-like particles from FFF 3-D printers during extrusion of ABS and PLA polymers that were composed of carbon and sometimes Fe, magnesium (Mg), and Si (Katz et al. 2020; Stefaniak et al. Stefaniak et al. 2019c; Youn et al. 2019). Oberbek et al. (2019) evaluated aerosol released during FFF 3D printing with a polymer that contained nanoscale hydroxyapatite (a calcium mineral) and noted release of spherical particles as well as particles with soot-like appearance that were composed of Al and carbon (but not calcium); the mean diameter of the soot-like agglomerates was 570 nm and the average diameter of the primary particles was 22 nm (Oberbek et al. 2019). Mendes et al. (2017) characterized particles released during extrusion of ABS and PLA polymers in a test chamber using a volatility tandem differential mobility analyzer, and consistent with the presence of organic compounds in printer aerosol emissions, observed that the aerosols were composed of low and high volatility constituents. Katz et al. (2020) utilized TEM with electron energy loss spectrometry (EELS) to discern the bonding state of elements in particulate released from FFF 3-D printers during extrusion of ABS polymer and identified carbon in π^* states formed from sp2-hybridized carbon, which is the bond state for compounds with aromatic ring structure.

Some investigators characterized the bulk chemistry of feedstock materials and aerosol released during FFF 3D printing. Zontek et al. (2017) analyzed the liquid phase aerosol released during extrusion of ABS polymer using attenuated total reflectance Fourier transform infrared spectroscopy and reported that it was composed of (tentative identification) cyclohexane, n-decane, ethylene-propylene-diene terpolymer, 1-decanol, and isocyanic acid. Katz et al. (2020) characterized the composition of particles released during extrusion of ABS polymer using an aerosol mass spectrometer and noted an elevated signal from aromatic derived ions (m/z = 77, 91, and 105) characteristic of polymeric styrene. Importantly, Katz et al. (2020) observed that the mass spectral results were preserved across particle sizes, which indicated that particle chemical composition was not size-dependent. Chýlek et al. (2019) performed thermogravimetric analysis (TGA) of 12 different types of polymers, including ABS, PLA, polyvinyl alcohol (PVA), co-polyester (CP), polycarbonate (PC), acrylonitrile styrene acrylate (ASA), nylon, and thermoplastic polyurethane (TPU) filaments and a TPU/PLA support material. Chýlek et al. (2019) reported that higher the total number of fine particles released, the greater the total weight of these particles and postulated that TGA may be suitable to estimate particle-phase emissions from polymer filaments to produce low-emitting filaments. Zisook et al. (2020) characterized aerosol released during extrusion of ABS polymer and found that particles had spherical shape (no soot-like clusters observed) with sizes from less than 100 nm to approximately 150 nm; some particles contained Ni, S, and chlorine (Cl). Zisook et al. (2020) also analyzed bulk samples of the ABS filament and reported that consistent with the composition of aerosol, the filament contained S at 852 ppm (0.0852% by wt.) and Cl at 99 ppm (0.0099% by

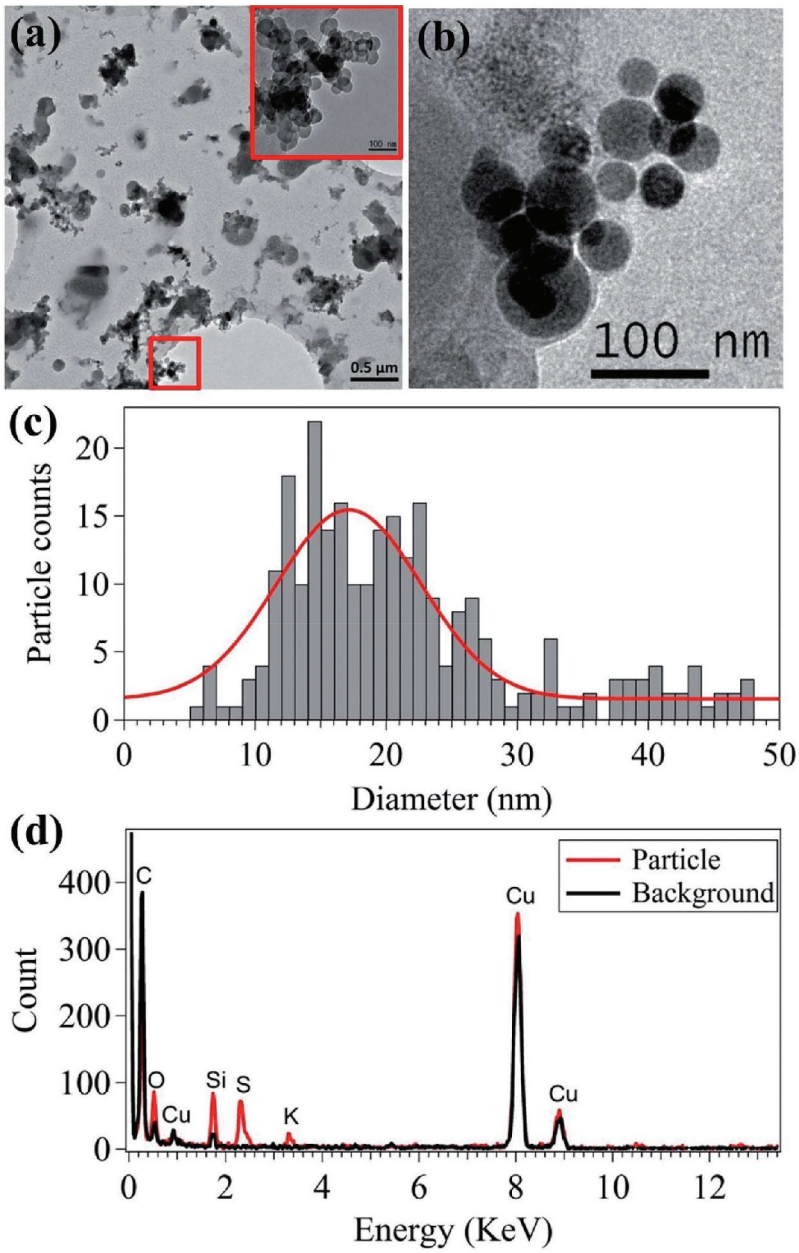

Figure 4. Morphology (a,b), size (c), and elemental composition (d) of soot-like cluster particles released during FFF 3-D printing. Reproduced under CC-BY-NC license from open access article by Youn et al. Characteristics of Nanoparticle Formation and Hazardous Air Pollutants Emitted by 3D Printer Operations: From Emission to Inhalation. *RSC Advances*. 9:19606–19612 (2019) – published by The Royal Society of Chemistry (Youn et al. 2019).

wt.). Results of these real-world studies are generally supported by observations from environmental test chamber evaluations of ME-type FFF 3D printers. Ding et al. (2019) noted that ultrafine particles released during printing with ABS and PLA were partially composed of VOCs. Gu et al. (2019) found that particles released during printing with ABS, ASA, high impact polystyrene (HIPS), polyethylene terephthalate glycol (PETG), and PC-ABS began to evaporate at 150°C and only 25% of particles (on a number basis) remained when heated to 300°C, which indicated that particles were largely composed of semi-volatile organic compounds (SVOCs). Wojtyla et al. (2020) characterized specific chemical constituents of bulk ABS and HIPS filaments using attenuated total reflectance Fourier transform infrared spectroscopy and compared these results to gas chromatography analysis of organic compounds evolved when pieces of the

same filament were heated to their printing temperature. ABS filaments contained methyl methacrylate, acrylonitrile, styrene, 1,2-butadiene, and 1,4-butadiene and evolved gases included methyl methacrylate, acrylonitrile, and styrene as well as several other organic compounds. For HIPS filaments, the dominant constituent was styrene, which was also quantified in evolved gas from the heated material (along with acrylonitrile, methylstyrene, cumene, ethylbenzene, toluene, 1-butanol, acetone, and/or, acetaldehyde). Vance et al. (2017) performed specific analyses of the chemical composition of bulk ABS and PLA filaments and aerosol released during FFF 3D printing. Interestingly, using Raman spectrometry, it was determined that the spectra for both the ABS filament and its printed part contained peaks for styrene and acrylonitrile; however, these peaks were absent from spectra of emitted particles, which suggested that these particles were not the result of volatilization and subsequent nucleation of ABS or direct release of ABS aerosols. The PLA filament was a copper-infused polymer that contained 21.1 ± 0.3% copper, though copper was not detected in particles emitted during printing. Yi et al. (2016) quantified the elemental composition of ABS and PLA filaments and compared these results to the composition of aerosol released during filament extrusion using children's 3D pen toys. Nine elements (Al, Ca, Co, Fe, Mg, Na, Ni, Si, and Zn) were quantified in the bulk filaments and in the aerosol; emission yields for elements ranged from 0.03 to 0.005 ng/g filament extruded (cobalt) to 127 to 3168 ng/g filament extruded (iron).

Factors that influence emissions

The release of particle- (Table 2) and gas-phase (Table 4) contaminants from ME-type AM machines was influenced by polymer type, number of printers in operation, extruder nozzle temperature, print step, filament feed rate, machine configuration (cover on, cover off), and printer status (normal operation, malfunction).

Stephens et al. (2013) first reported polymer-dependent differences in particle number-based ERs; the value for ABS was higher than for PLA. Subsequently, investigators have measured emissions from a broader array of polymer types used in FFF 3-D printers and reported polymer-dependent differences (Chýlek et al. 2019; McDonnell et al. 2016; Stabile et al. 2017; Stefaniak et al. 2019c). For example, in one study, particle number-based ERs ranged from 10^6 #/min (PLA, PVA, TPU/PLA) to 10^9 #/min (ABS, ASA, PC, nylon); corresponding number-based yield values were 10^7 #/g polymer extruded (PLA, PVA), 10^8 #/g printed (support material, TPU/PLA), 109 #/g printed (CP), and 10^{10} #/g polymer extruded (ABS, ASA, PC, nylon) (Chýlek et al. 2019). A recent environmental test chamber study indicated that the presence of metal additives in feedstock filament resulted in higher number-based emission rates compared with neat filaments of the same polymer type without metals (Alberts et al. 2021). Mass-based particle ERs from a desktop scale-FFF 3D printer using ABS and PLA ranged from 2.8 to 7.3 μg/min (Katz et al. 2020). For industrial-scale FDM™ machines, particle number-based ERs were higher during extrusion of ABS and PC (2.2 x 10^{11} #/min) compared with Ultem® (4.1 x 10^{10} #/min) (Stefaniak et al. 2019b). Dunn et al. evaluated workplace emissions in a facility that extruded poly ether ether ketone (PEEK) filament and PEEK filament with carbon nanotube (CNT) or carbon nanofiber (CNF) additives using filter-based sampling and a thermophoretic precipitator to directly capture particles onto a microscopy grid. From TEM analysis, polymer particles that contained CNFs and CNTs were present in all filter samples and free (unbound) CNT, free CNF, and polymer particles that contained CNFs and CNTs were identified in grid samples (Dunn et al. 2020a). The observation of polymer particles that contained CNTs is consistent with the results of an environmental test chamber evaluation of particle emissions from FFF 3-D printers during extrusion of ABS, PLA, and PC filaments that contained CNTs (Stefaniak et al. 2018).

Gas-phase emissions were also influenced by feedstock polymer type. In one study, average and peak TVOC concentrations were (from highest to lowest): nylon = PC > ABS = PLA (McDonnell et al. 2016). In another study, the rank order of TVOC concentrations was: ABS (391 μg/m^3) > PLA (255 μg/m^3) > polyethylene terephthalate (PET, 155 μg/m^3) (Bravi, Murmura, and Santos 2019). For a room with seven printers extruding ABS and PLA simultaneously, the TVOC ER was 3300 mg/min. For a sheer printer (hybrid FFF

printer and inkjet printer) that extruded PLA to create channels that were filled with silver ink, TVOC ERs (16 to 31 mg TVOC/min) were similar to desktop-scale FFF 3-D printers using PLA only (2 to 44 mg TVOC/min) (Stefaniak et al. 2019c). TVOC ERs for industrial-scale FDM™ machines ranged from 19 (ABS and PC) to 94 mg TVOC/min (Ultem®), which is similar to desktop-scale FFF 3-D printers (Stefaniak et al. 2019b). Väisäinen et al (2019) reported that levels of formaldehyde and acetone were similar for PLA filaments with wood additive (EasyWood™) or carbon fiber additive, but lower than from ABS with flame retardant additive. In that same study, there were measurable concentrations of 23 individual VOCs released from EasyWood™, 20 individual VOCs released from PLA with carbon fiber additive, and 38 individual VOCs released from ABS with flame retardant additive. The five VOCs present at the highest average mass concentrations at the midpoint of the print jobs are presented in Table 4. In another study, the concentrations of individual VOCs inside the build chamber of a desktop-scale FFF 3D printer were measured and concentrations differed by polymer type, e.g., the rank order for styrene was ABS (69 μg/m^3) > PLA (21 μg/m^3) > PET (6 μg/m^3). The authors suggested it might be possible to identify a "fingerprint" of VOC emissions for each type of polymer based on the percent mass accounted for by the major released substances (Bravi, Murmura, and Santos 2019). For industrial-scale FDM™ machines, six different VOCs (acetone, benzene, styrene, toluene, *m, p*-xylene, and o-xylene) were measured in workplace air. During extrusion of ABS and PC, the concentration of acetone ranged from 5700 to 3.3 × 10^4 μg/m^3 whereas during extrusion of Ultem® it was 400 μg/m^3 (Stefaniak et al. 2019b). Pinheiro et al. (2021) developed an optoelectronic nose and used it to identify VOCs emitted from ABS, PLA, and PETG filaments. Paper dye-based sensors were fabricated and placed inside the build chamber of an FFF 3D printer. Major VOCs identified during printing with ABS were styrene, cyclehexanone, isobutanol, and ethylbenzene, for PLA were isobutanol, methyl methacrylate, acetone, and lactide and for PETG were toluene, formaldehyde, and acetone (Pinheiro et al. 2021). Finally, it is interesting to note that results of an environmental test chamber study indicated that CNT additives in an ABS filament acted as a trap that lowered the total level of organic compound emissions under most experimental conditions; however, they elevated the emission levels of several hazardous VOCs, including α-methylstyrene and benzaldehyde (Potter et al. 2019).

Particle number concentration in indoor air increases as the number of FFF 3D printers in operation increases (Bharti and Singh 2017; Youn et al. 2019). In addition, inhalable mass concentration in a room rose from 300 to 700 μg/m^3 as the number of desktop-scale FFF 3D printers in operation increased, though respirable mass concentration was reported to be higher for one printer (800 μg/m^3) compared with three printers (400 μg/m^3). In that same study, isopropyl alcohol, acetone, ethanol, and TVOC concentrations were higher when three printers were in operation compared with one printer (Chan et al. 2020).

The temperature of the extruder nozzle has a major impact on emissions (Deng et al. 2016; Mendes et al. 2017; Stabile et al. 2017). As presented in Table 2, Stabile et al. (2017) extruded ten different filaments on a FFF 3D printer and reported that particle number-based ERs and alveolar lung deposited particle surface area (LDSA) dose rose as nozzle temperature increased from 180°C to 240°C. These nozzle temperatures spanned the range recommended by the filament manufacturer for PLA Wood 1, Flex PLA, CP, CP with carbon fiber, and nylon but as noted by the authors, some temperatures that were tested exceeded the filament manufactures recommendations for PLA, PLA Wood 2, PLA with copper, PLA with bamboo, and Ninja Flex®.

Typically, a rapid "burst" in particle concentration is observed at the start of an ME-type print job followed by a slower decay through the end of the last build cycle. To better understand this observation, using ABS and PLA, Deng et al. evaluated the print process in four steps: 1) load a filament into the extruder nozzle, 2) heat the extruder nozzle and/or build platform to the desired temperature for the specific polymer type, 3) print a part, and 4) unload any unused filament from the extruder nozzle (Deng et al. 2016). For ABS, particle emissions were highest during step 2 (see Figure 5). During this step, the extruder nozzle reached its set temperature (200°C to

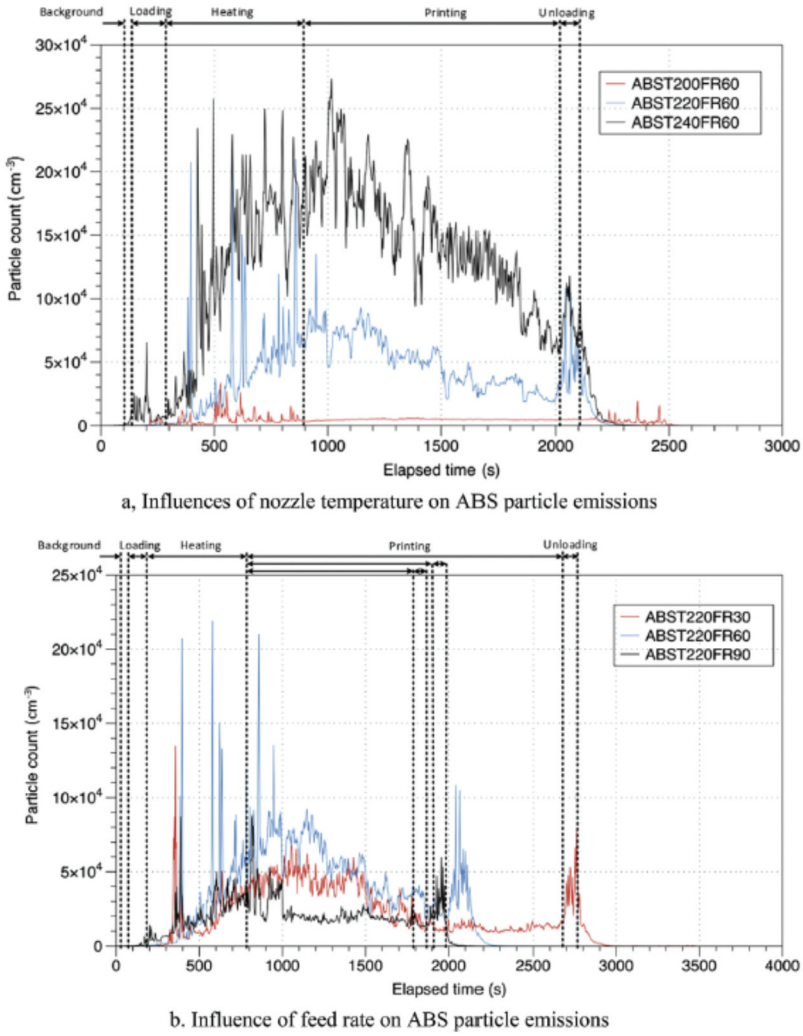

Figure 5. Increases in particle number concentration during heating step of print process for ABS polymer at nozzle temperatures (T) of 200, 220, and 240°C and constant filament feed rate (FR) of 60 mm/min (top panel) and at filament FRs of 30, 60, and 90 mm/min and constant nozzle T of 220°C (bottom panel). Reproduced with permission from Deng et al. The impact of manufacturing parameters on submicron particle emissions from a desktop 3D printer in the perspective of emission reduction. *Build Environ*. 104:311–319 (2016) – published by Elsevier (Deng et al. 2016).

240°C, depending on the test) in a few minutes but the build platform required 10 minutes to reach its set temperature (110°C for all tests). As a result, the filament underwent thermal decomposition in the hot extruder nozzle while the build platform heated. This effect was not detected for PLA at extruder nozzle temperatures of 180°C to 220°C because the build platform took approximately one min to reach its set temperature of 60°C so the residence time of the filament inside the extruder was shorter (Deng et al. 2016). Subsequent reports confirmed that the rapid increase in particle number concentration at the start of printing was related to the prolonged filament residence time in the extruder nozzle during the heating step, not the print step because during printing the filament residence time in the nozzle was just a few seconds (Chýlek et al. 2019; Simon, Aguilera, and Zhao 2017). Simon, Aguilera, and Zhao (2017) in a follow-on to their field study conducted experiments in an environmental test chamber and reported that particle emissions were highest from the start of the print job through the completion of the raft (layers of disposable polymer deposited onto the build platform to enhance adherence of the part to the platform), decayed to baseline while the sides of an object were printed, and increased steadily while the infill (repeated structure with defined pattern and density that fills the interior

space of a part) was printed. In another environmental test chamber study, Bernatikova et al. (2021) demonstrated that particle number concentration rose rapidly during printer extruder nozzle heating and peaked during printing for PETG and styrene-free CP filaments. Oberbek et al. (2019) assessed particle number concentration and LDSA for six production events (turning on the 3D printer, backfilling nanocomposite granulate, starting printing, workers moving around the room, processing, checking devices, and ending the print process) during FFF 3D printing with a hydroxyapatite composite. Inside the partial enclosure surrounding the printer, particle number concentration did not exceed background for any event; LDSA values ranged from 0.26 to 0.64 $\mu m^2/cm^3$. In the room, particle number concentration only exceeded background during processing events (404 to 495 $\#/cm^3$); LDSA values were 0.57 to 0.62 $\mu m^2/cm^3$ during these events. The respirable mass concentration reported was just 0.02 $\mu g/m^3$ (Oberbek et al. 2019).

Filament feed rate has been shown to influence the release of contaminants from desktop-scale FFF 3D printers to indoor air (Chýlek et al. 2019; Deng et al. 2016; Simon, Aguilera, and Zhao 2017). As illustrated in Figure 5, for ABS and (to a lesser extent) PLA filaments, a feed rate of 60 mm/min resulted in higher particle number concentrations in a room compared with feed rates of 30 or 90 mm/min (Deng et al. 2016).

Many FFF 3D printers were designed with loose fitting covers, walls, and doors that enclosed the build chamber but were not sealed for emissions containment. Zontek et al. (2017) measured the concentration of particles inside and outside of the enclosure of a desktop-scale FFF 3D printer and reported a 95% reduction in particle number concentration and 99% reduction in particle mass concentration during printing. Consistent with this observation, results from multiple workplace assessments demonstrated that particle concentrations in indoor air increased when a printer cover was removed and decreased when it was replaced (Du Preez et al. 2018b; Stefaniak et al. 2019c; Yi et al. 2016). Note that even with a cover in place, during operation of desktop-scale FFF 3D printers, the particle concentration in many indoor workspaces is on the order of 10^4 to 10^5 $\#/cm^3$ (Du Preez, de Beer, and Du Plessis 2018b; Yi et al. 2016).

Generally, desktop-scale FFF 3D printers do not have a feedback mechanism that turns off the extruder nozzle when the filament becomes jammed or there is a print error. As a result, filament in the extruder nozzle continues to be heated though the machine is not printing. Particle number concentration and LDSA dose, as well as TVOC concentration, were found to increase when a FFF 3D printer malfunctioned compared with normal operation (Mendes et al. 2017; Stefaniak et al. 2019c; Väisänen et al. 2019).

Factors that influence exposures

No apparent data on exposures incurred during ME pre-printing tasks such as loading filament into a printer and cleaning printer surfaces were identified in the literature. Available data on personal exposures during ME printing, post-printing, and post-processing tasks are summarized in Table 3 and Table 5 for particle- and gas-phase contaminants, respectively. Du Preez et al. (2018b) measured PBZ exposures of workers that extruded ABS and PLA polymers on desktop-scale FFF 3-D printers and ABS and PC polymers on industrial-scale FDM™ machines. The employee using FFF 3-D printers had exposures to low levels of Al (10 $\mu g/m^3$ compared to its NIOSH Recommended Exposure Limit (REL) of 10,000 $\mu g/m^3$) and acetone (300 $\mu g/m^3$ compared to its NIOSH REL of 590,000 $\mu g/m^3$) (NIOSH 2007). The employee using industrial-scale FDM™ printers had exposure to acetone that ranged from 290 to 7210 $\mu g/m^3$ (Du Preez et al. 2018b). In another study, the same research group measured PBZ exposures to VOCs for workers that performed FFF 3D printing with ABS and PLA polymers (Stefaniak et al. 2019c). Employees working with ABS were exposed to up to six different VOCs; the highest PBZ exposures were to acetone and naphtha (mixture of hydrocarbons), though the latter was not attributed to the 3D printing process. For employees that printed with PLA, up to eight different VOCs were quantified in the PBZ; concentrations ranged from 0.6 $\mu g/m^3$ for methylene chloride (categorized as a carcinogen by NIOSH with no REL) to approximately 9800 $\mu g/m^3$ for isopropyl alcohol (RELs of = 980,000 $\mu g/m^3$). In a separate study of industrial-scale FDM™ machine operators, employees that extruded ABS and PC polymers had low level

exposures to Al and Fe (NIOSH REL = 5000 μg/m^3) that did not exceed 10 μg/m^3. Employees that extruded ABS, PC, and Ultem™ polymers had exposure to acetone (40 to 1880 μg/m^3), pentane (40 to 110 μg/m^3), cyclohexane (10 to 40 μg/m^3), ethanol (30 to 80 μg/m^3), and naphtha (2000 to 2300 μg/m^3), all of which were below their respective NIOSH RELs. In addition, low exposures of hexane (150 to 190 μg/m^3 compared with the NIOSH REL of 180,000 μg/m^3 and benzene (20 to 30 μg/m^3 compared with the NIOSH REL for this carcinogen of 319 μg/m^3) were measured in the PBZ during extrusion of ABS and Ultem™, but not PC polymer (Stefaniak et al. 2019b). Dunn et al. (2020a) evaluated PBZ exposures at a facility that extruded PEEK polymer and PEEK polymer with CNT or CNF additives. TEM analysis of filter samples identified polymer particles that contained CNFs and CNTs in all samples. Free CNTs (unbound to polymer) were observed on one sample (Dunn et al. 2020a).

FDM™ machines have an enclosed build chamber to maintain a stable thermal environment during polymer extrusion. Once the last build cycle is completed, an operator must open the machine doors to retrieve the printed parts. Du Preez et al. (2018b). positioned a real-time CNC and a photoionization detector (PID) in the PBZ of an employee when doors to three industrial-scale FDM™ machines were opened. Each machine extruded a different polymer and builds were completed 16.5 (ABS), 1.75 (PC), and 23.2 (Ultem®) hours prior. Upon opening, particle number concentrations were relatively stable and low but peaks in TVOC concentrations of 1.7 x 10^4, 1600, and 3600 μg/m^3 were observed for ABS, PC and Ultem®, respectively (Du Preez et al. 2018b).

It is rare that a finished product can be entirely manufactured within a single process, and AM is no exception (ISO/ASTM 2015). As such, post-processing is often required to achieve a finished product. For parts made from ABS polymer, acetone is used to vapor polish to achieve a smooth glossy surface appearance. For parts made from PLA polymer, chloroform is used to vapor polish. Du Preez et al. (2018b) measured PBZ exposures to metals for employees that extruded ABS and PLA polymers on desktop-scale FFF 3D printers and performed AVP and CVP tasks. During printing and AVP, personal exposures to metals were 10 μg/m^3 for Fe and 20 μg/m^3 for Al. When an employee dispensed acetone into the polishing chamber using a syringe, the TVOC concentration in the room rapidly increased to 9 × 10^5 μg/m^3. Once the chamber was sealed, the TVOC concentration in the room returned to background levels within 20 min. When the chamber was opened to retrieve the polished part, the TVOC concentration in the room again rose steeply to approximately 9 × 10^5 μg/m^3. For the AVP task, six VOCs were quantified on PBZ samples; concentrations of acetone ranged from 380 to 6470 μg/m^3. CVP was performed outdoors. When the employee poured chloroform onto a brush, the TVOC concentration increased to 2.4 × 10^5 μg/m^3 and was 1 × 10^5 to 2 × 10^5 μg/m^3 while brushing the part. The employee's PBZ exposure to chloroform during this task was 180 μg/m^3 (60-min REL of 978,000 μg/m^3). Freiser et al. (2018) examined PBZ exposures to dust and VOCs during drilling of medical models of temporal bones that were printed using ABS or PLA polymers. The drill had a suction irrigator at the tool-part interface and levels of dust and VOCs were below their respective analytical LODs. Dunn et al. (2020a) reported that particle concentrations in a manufacturing area rose to approximately 1.5 × 10^5 #/cm^3 when an employee cut parts made of PEEK polymer using a rotary tool.

Room ventilation influences emissions and exposures. Steinle (2016) determined emissions from a desktop-scale FFF 3D printer during extrusion of PLA in a 180 m^3 room with 2 air changes/hr (ACH) of general exhaust ventilation and a 30 m^3 unventilated room. Particle number concentration, respirable and inhalable dust concentrations, TVOC concentration, and methyl methacrylate concentration were all higher in the unventilated room compared with ventilated room. Zontek et al. (2017) examined emission from a desktop-scale FFF 3D printer during extrusion of PLA in a 600 m^3 lab with 20 ACH and from another FFF 3D printer during extrusion of ABS in a 162 m^3 room with 1.8 ACH. Particle mapping demonstrated a concentration build up throughout the 162 m^3 room but concentration remained localized around the printer in the 600 m^3 lab, which indicated the potential for higher exposures in the room with less general exhaust ventilation (Zontek et al. 2017).

Material jetting

Four studies were identified on the emissions from MJ machines (Ryan and Hubbard 2016; Stefaniak et al. 2019b; Väisänen et al. 2019; Zisook et al. 2020). These studies reported measurements from five different workplaces, which included an office and industrial workplaces. Among workplaces, room characteristics ranged from a 48 m^3 office (ACH not reported) to a 466 m^3 research lab (2 ACH). Particle number-based ERs measured using CNCs ranged from 1.5×10^9 #/min to 2.3×10^{10} #/min, but rates based upon mobility particle sizer measurements were up to 2.1×10^{12} #/min. TVOC ERs were reported to be 2.5×10^4 mg/min to 4.5×10^4 mg/min. One study determined PBZ monitoring results for metals and another PBZ exposures to organic gases.

The first study, by Ryan and Hubbard (2016) measured particles and VOCs inside a build chamber during printing with liquid (Object VeroWhitePlus) feedstock resin. Particle mass concentration ranged from 3 μg/m^3 (particulate matter with aerodynamic diameter less than 10 μm (PM_{10}) outside the printer) to 30 μg/m^3 (particulate matter with aerodynamic diameter less than 1 μm (PM_1) inside the printer), with PM_1 decreasing and $PM_{2.5}$ rising during printing (Table 2). Acetone, n-butanone, 2-butanone, 1,4-dioxane, ethanol, isopropyl alcohol, and toluene were determined in the room (Table 4). 1,4-Dioxane, a potential occupational carcinogen (NIOSH 2007), was present at the highest concentration (100 μg/m^3); none of the other six VOCs exceeded 14 μg/m^3 (Ryan and Hubbard 2016).

Stefaniak et al. (2019b) evaluated emissions at two AM facilities, both of which used the same model of industrial-scale MJ machine. Both facilities used TangoBlack+ and VeroClear resins and VeroWhite+ resin was also used at the second facility. Particle number-based ERs (20 to 1000 nm size range) were 1.5×10^9 #/min (printer lid closed) to 2.3×10^{10} #/min (printer lid open). ERs for particles in the 5.6 to 560 nm size range were higher, up to 2.1×10^{12} #/min (lid closed). The higher ERs calculated from the particle counting instrument with lower size cutoff of 5.6 nm compared with the instrument with lower size cutoff of 20 nm, indicated that a significant number of particles were between 5.6 and 20 nm. ERs of particles in the 0.3 to >20 μm size range were 8.5×10^3 #/min (lid closed) to 1.1×10^5 #/min (lid open). Scanning electron microscopy (SEM) analysis showed clusters of ultrafine particles and EDX analysis revealed that the particles were composed of carbon. TVOC ERs were 4.5×10^4 μg TVOC/min (lid closed) to 2.5×10^4 μg TVOC/min (lid open) and were not influenced by the lid position. Among individual VOCs quantified, with the exception of acetaldehyde (14 to 214 μg/m^3), none of the compounds (acetone, benzene, ethanol, toluene, and *m, p*-xylene, or *o*-xylene) exceeded 1.4% of their respective NIOSH REL. Ethanol was used to clean the build platform of the machine prior to operation at one facility and the area monitoring concentration was 10,600 μg/m^3, which indicated that non-printing tasks also contributed to room contaminant levels. MJ machine operators' PBZ exposures to VOCs at one facility included acetone (20 to 80 μg/m^3), ethanol (520 to 2020 μg/m^3, REL = 1,900,000 μg/m^3), isopropyl alcohol (70 to 520 μg/m^3), naphtha (1530 to 1710 μg/m^3, REL = 400,000 μg/m^3), and pentane (10 to 60 μg/m^3) (Stefaniak et al. 2019b).

Väisänen et al. (2019) characterized emissions and indoor air quality (IAQ) parameters during MJ printing and post-processing tasks using a transparent/clear liquid photopolymer resin (3D systems, VisiJet M2R-CL). Post-processing involved ultrasound treatment while submerging the manufactured part in a water container. No increase in particle number concentrations was evident during printing (mean ± SD: 980 ± 90 #/cm^3) compared with background (1050 ± 50 #/cm^3). Dust concentrations measured on filter samples never exceeded 30 μg/m^3 during printing (Table 2). TVOC and individual VOCs levels were measured for the printing and post-processing tasks (see Table 4). The mean TVOC level during printing was 2496 μg/m^3 compared with 1809 μg/m^3 during post-processing. Thirty-one different VOCs were quantified in air during printing, including isobornyl acrylate (1325 to 2076 μg/m^3), 2-furanpropanoic acid (127 to 164 μg/m^3), aromatic hydrocarbons, butylated hydroxytoluene, xylenes, toluene and ethylbenzene (between 22 to 113 μg/m^3). The same VOCs were prominent during post-processing as well as styrene (33 μg/m^3). No short-chained carbonyl compounds were

detected during printing. The high TVOC and individual VOC concentrations might be attributed to aerosolization of the liquid feedstock that is jetted through a feeder nozzle at high pressure during printing. Carbon monoxide (CO) concentrations, although very low, increased during printing to an average of 0.5 ppm (background mean = 0.1 ppm), while carbon dioxide (CO_2) concentrations averaged 560 ppm (background mean = 540 ppm) (Väisänen et al. 2019).

Finally, Zisook et al. (2020) investigated particle and VOC emissions during MJ printing (8 hr) and post-processing tasks (80 min). The feedstock resin contained glycerin and acrylate compounds. Post-processing tasks involved transfer of the printed parts to a rinsing cabinet for cleaning with soapy water followed by rinsing in either a lye bath or sink. No particle emission data was reported, and the authors only indicated that emissions were either not detected or were very low. TVOC concentrations were not distinguishable from background concentrations during MJ printing nor post-processing tasks. Of the 61 VOCs and 9 other compounds sampled for in this study, only toluene was detected in one sample during printing at a concentration above background (mean = 27 $\mu g/m^3$). Isopropanol (mean = 656 $\mu g/m^3$) and propylene (15 $\mu g/m^3$) were detected during printing and isopropanol (492 $\mu g/m^3$) was quantified during post-processing; however, concentrations were lower than in the background. According to Zisook et al. (2020) isopropanol may not represent emissions from the MJ machine and were associated with other products used elsewhere in the facility. No marked differences were found between levels of VOCs measured inside or outside of the machine (Zisook et al. 2020).

Powder bed fusion

Published literature associated with PBF was mainly focused on environments that utilize metals as feedstock materials. Of the 15 published articles related to PBF, 11 focused on metal feedstocks and 4 on nylon polymers. Numerous studies conducted static area monitoring using a variety of direct reading instruments in manufacturing facilities, government research institutes, and university lab settings. Room volumes ranged from 117 m^3 (university lab, ACH not reported) to 1176 m^3 (manufacturing facility, ACH not reported). Average particle number concentrations (CNC data) during PBF and related tasks ranged from 1100 #/cm^3 to 1.7×10^4 #/cm^3; one study reported a particle number-based ER of 2.8×10^{10} #/min. Many investigators used real-time instruments to measure particle mass concentration; mean values measured using a laser scattering photometer (LSP) were 39 to 1.5×10^5 $\mu g/m^3$. TVOC concentrations during PBF with nylon powder were 113 $\mu g/m^3$ to 1285 $\mu g/m^3$. Four investigations of PBF processes that use metal powders included PBZ air monitoring for elements. No PBZ measurements for organic gases were found in the literature. Microscopic techniques have been used to conduct particle characterization of workplace air; only 6 of 15 studies investigated personal exposures.

Static area monitoring

Throughout the investigation of particle number concentrations measured during all PBF process phases, peak concentrations were predominantly observed during manual tasks performed by the AM operator (Beisser et al. 2017; Graff et al. 2017; Kolb et al. 2017; Ljunggren et al. 2019; Walter et al. 2018). Graff et al. (2017) found that peak particle number concentration in the 10 to 300 nm size range was 1.6×10^4 #/cm^3 for the task of cleaning a PBF machine and concluded that the generation of particles smaller than 300 nm was limited in this AM workplace. Graff et al. (2017) also measured particles in the 300 nm to 10 µm size range and notted that peak particle number concentrations at the locations where machine opening, vacuuming and handling the build platform, sieving, cleaning, and filling the machine with powder tasks were performed ranged from < 50 #/cm^3 to just over 100 #/cm^3. Numerous studies thereafter demonstrated that elevated particle concentrations were usually most evident during post-printing tasks with metals such as Inconel 781, Ti64, $AlSi_{10}Mg$, and martensitic stainless steel. Post-printing tasks included machine opening, cleaning of the AM machine, powder refilling, part (build) removal and removal of excess powder (Kolb et al. 2017; Ljunggren et al. 2019; Philippot et al. 2020; Walter et al. 2018). Three studies (Damanhuri et al. 2019a,

2019b; Zisook et al. 2020) investigated emissions of nylon-12 (PA 2200) during SLM/SLS PBF and one study examined emissions from a glass reinforced nylon (polyamide) powder feedstock (Väisänen et al. 2019). Two of these studies were carried out at the same facility but on different occasions, and included real-time monitoring of respirable particles, TVOC, and CO_2 concentrations (Damanhuri et al. 2019a, 2019b). Particle number concentrations and CO_2 concentrations were the highest during the pre-printing phases of both the studies. Powder weighing, mixing, and loading into the machine had the highest value of respirable particles (as $PM_{2.5}$) at 1450 μg/m^3. Formaldehyde was measured but no significant differences were detected during the different process phases. Overall, for TVOC, the highest peak values occurred during the post-printing phase and ranged from 1150 to 1600 μg/m^3 (Damanhuri et al. 2019b).

Väisänen et al. (2019) reported on PBF and multi-jet fusion (MJF) printer emissions while using glass reinforced nylon powder. MJF is similar to SLM/SLS as it also utilzes powdered feedstock polymers; however, rather than using a laser to sinter or melt the powder material, MJF uses a fusing agent and a detailing agent to bond the powders by infrared radiation (Wu et al. 2020). During post-printing, dust concentrations ranged from 0.1 to 2.57 mg/m^3 (measured using a DustTrak™ instrument); stationary samples reached a peak of 5200 μg/m^3 during PBF. Particle concentrations (1.5 x 10^4 to 2.2 × 10^4 #/cm^3) exceeded background levels. Although the measured TVOC concentrations were very low during PBF, formaldehyde was detected at 40 μg/m^3. Relatively higher VOC concentrations were detected during MJF where a pressurized spray of binding chemicals was used; the mean TVOC concentration of 1114 μg/m^3 was almost three-fold higher compared with background (Väisänen et al. 2019). Evidence indicated that the use of binding chemicals during printing reduced the formation of airborne particles; however, dust concentrations measured during MJF was of the same magnitude as concentrations from PBF post-printing. Zisook et al. (2020) found that mean total dust concentrations (measured using a DustTrak™ instrument) were 400 μg/m^3 during the PBF post-print phase. Further, respirable and total particle concentrations exceeded background during powder handling and parts processing but were below applicable American Conference of Governmental Industrial Hygienists (ACGIH®) Threshold Limit Values (TLVs®); inorganic gases were not detected.

Numerous metal powders are commercially available for PBF manufacturing that consist of a variety of elements such as Al, Cr, cobalt (Co), copper (Cu), Fe, Mn, and Ti. Stationary air monitoring by Graff et al. (2017) indicated the presence of Cr (21 μg/m^3 to 50 μg/m^3), Ni (48 μg/m^3 to 110 μg/m^3) and Co (13 μg/m^3 to 42 μg/m^3). Most investigators reported that detectable levels of metals were measured and complied with their specified OELs (Beisser et al. 2017; Kolb et al. 2017; Ljunggren et al. 2019). Beisser et al. (2017) measured respirable and inhalable dust fractions of individual metallic elements for stainless steel and Ni-, Al-, Ti-, and Co-based alloys; metal concentrations were highest during post-processing (grinding, abrasive blasting). Cr(VI) was not detected in air when materials containing Cr were used. Gomes et al. (2019) employed stationary monitoring at operator workstations and noted peak particle number concentrations of 1.8 × 10^4 #/cm^3 along with LDSA values of 457 μm^2/cm^3. Jensen et al. (2020) examined several tasks and found that grinding led to the highest rise in particle number concentrations of 2.5 × 10^5 #/cm^3 and also led to LSDA values of 79.3 μm^2/cm^3; particle sizes were generally less than 200 nm.

Particle characterization

Metal powder feedstock can be used as virgin (new, as provided by the manufacturer) or recycled (blend of used and virgin) powder. Several studies characterized both new and used metal feedstock powders. Mellin et al. (2016) investigated formation of nanoscale particle byproducts during PBF SLM/SLS processing using Inconel 939 (Ni, Cr, and Co alloy). From SEM images, small spherical particles (called "satellites") were observed in the recycled powder. Satellite particles (1.2 μm to 5.8 μm) became attached to larger particles (23.4 μm) during the processing phase and it was hypothesized these could detach from larger particles during

powder handling. Although personal monitoring of AM operators was not performed, it was found that small respirable metal particles (~1 μm to 2 μm) were generated during processing (Mellin et al. 2016). Graff et al. (2017) also investigated Inconel 939 powder but analyzed the feedstock using laser diffraction analysis to determine particle volume and number percentages. The powder supplier indicated that the powder particles were in the range of 15 μm to 45 μm; however, observed particle sizes were much smaller (<10 μm). Sutton et al. (2020) examined stainless steel 304 L powder and confirmed morphological, microstructural, and surface chemistry differences between virgin and recycled powders used during SLM/SLS processing. Recycled powder consisted of a combination of laser spatter and condensate, and similar to Mellin et al. (2016) aggregates were found in the recycled powder indicating that vaporization of all elements occurred during SLM/SLS processing. In a study by Du Preez, de Beer, and Du Plessis (2018a) three different titanium alloy powders (virgin and recycled) used in PBF AM, together with their relevant safety data sheets (SDSs) were investigated. Feedstock powder was analyzed in terms of particle size, shape, and elemental composition. The results indicated that thoracic (<10 μm) and respirable (<4 μm) sized metal-containing particles were present in the virgin and recycled powders. Consistent with Graff et al. (2017) Du Preez, de Beer, and Du Plessis (2018a) also noted discrepancies in particle size and elemental composition compared with what was declared in the SDSs.

Damanhuri et al. (2019a) characterized nylon-12 (polyamide) powder used during PBF SLM/SLS. The powder particles were relatively uniform sphere-shaped with size of 60 μm, which enabled the uniform spread of powder during SLM/SLS printing. Gomes et al. (2019) employed TEM-EDX for the analysis of stainless steel 316 L powder and specified the presence of nanoparticles, apart from some more coarse particles that were ascribed to the presence of unmelted powder particles. The powder composition was Fe, Si, Mn, S, and phosphorus (P), which are the main elements present in steel (Gomes et al. 2019).

SEM analysis of virgin and used Hastelloy® (Ni, Cr, Fe, Mo, and Co) powder revealed particles in the size range of 4 to 10 μm; recycling of the powder caused fragmentation of particles to smaller sizes (Ljunggren et al. 2019). Agglomerates were present in recycled powder that were composed of ultrafine particles (d < 100 nm) attached to larger particles. EDX analysis revealed that ultrafine particles in the recycled powder contained similar elements as the virgin powder. Sodium (Na) and S were only found in ultrafine particle agglomerates from the recycled alloy powder. Philippot et al. (2020) provided a broad overview of several investigations that included PBF with different metal-based powders, though the authors did not specify the specific types of powders in their report. All SEM observations were in accordance with previous studies, i.e., there were morphological differences between the virgin and recycled powders with the presence of aggregated/agglomerated nanoscale particle in the recycled powders (Du Preez, de Beer, and Du Plessis 2018a; Mellin et al. 2016; Sutton et al. 2020).

Personal exposure monitoring

Graff et al. (2017) conducted personal exposure monitoring for 45 min during PBF tasks that included opening an AM machine, vacuuming the build/base plate, handling of the build/base plate, sieving metal powder, cleaning an AM machine, and filling an AM machine with metal powder (Table 3). Personal exposure monitoring of operators to inhalable metals confirmed exposure to dust (210 $\mu g/m^3$), Cr (< 44 $\mu g/m^3$), Ni (< 99 $\mu g/m^3$), Co (< 38 $\mu g/m^3$), and Fe (< 100 $\mu g/m^3$). Graff et al. (2017) did not perform time weighted average (TWA) calculations, and therefore, could not compare exposure to Swedish legislative OELs of the individual metals. In another study, AM operator's personal exposure to Inconel 718 and Ti64 powders were investigated simultaneously to determine their exposures during different AM tasks (Ljunggren et al. 2019). The results from the inhalable and respirable particle fractions from personal sampling indicated that AM operators were exposed to detectable levels of Ni, Cr, Fe, and Ti, though background values were higher compared with the inhalable fraction. All personal exposure data complied with their respective Swedish OELs, except one AM operator's personal inhalable exposure to Co (28.3 $\mu g/m^3$). Their study compared the

AM environment to a welding environment and concluded that metal powder components were more evident in the AM environments.

Jensen et al. (2020) investigated emissions from Ti6Al4V during different AM-related activities, which included cleaning and opening/closing an SLM/SLS printer and grinding. In this study, the respirable mass concentrations of airborne particles were 20 μg/m^3, which was below the 8-hour TWA OEL in Denmark.

Ljunggren et al. (2019) was the first to examine biomonitoring of urine and dermal contamination of AM operators during the PBF process. Data demnstrated that AM operators displayed detectable dermal exposure to Co (110 ng/cm^2), Ni (630 ng/cm^2), and Cr (370 ng/cm^2) on the index finger of their dominant hand. Participants with the highest levels of Co on their hands were the same individuals with the highest level of Co in urine. The biomonitoring results showed a non-significant increase in the level of Co (4.7 to 7.3 nmol/L), Ni (23.2 to 33.0 nmol/L), and Cr (1.3 to 1.8 nmol/L) in the urine of the AM operators at the end of the work week compared with controls (Ljunggren et al. 2019). Väisänen et al. (2019) found personal inhalable dust concentrations up to 9100 μg/m^3 (PBF) and 2400 μg/m^3 (MJF) during post-processing of glass reinforced nylon-12 powder.

Sheet lamination

No apparent reports in the peer-reviewed literature on emissions or exposures from SL processes were identified.

Vat photopolymerization

Four studies reported particle and VOC emissions and exposures during VP printing and post-processing tasks (Freiser et al. 2018; Väisänen et al. 2019; Yang and Li 2018; Zisook et al. 2020). Of these studies, only one monitored real-time particle concentrations in a 55 m^3 apartment (ACH not reported) where the VP printer was operated; average particle number concentration (CNC data) was 8020 #/cm^3 and mean particle mass concentration (LSP data) was 50 μg/m^3. Organic chemical emissions were measured in a medical lab (room volume and ACH not reported), apartment (55 m^3, ACH not reported), university room (155 m^3, ACH not reported), university research lab (41 m^3, ACH not reported), and industrial lab (28 m^3, ACH = 8.6). Various sampling and analytical techniques were used to determine TVOC concentrations; values ranged from 84 μg/m^3 to 1053 μg/m^3 during printing and from 1774 μg/m^3 to approximately 11,000 μg/m^3 during part washing. No PBZ monitoring data for elements were reported in the literature and one study reported PBZ monitoring for isopropyl alcohol.

Freiser et al. (2018) measured personal exposures to particles and VOCs during high-speed surgical drilling of temporal bone models manufactured from photoacrylic resin (a mixture of methacrylic acid esters and photoinitiator). Total particle mass concentrations did not exceed the LOD of 1.4 μg/m^3 and the only VOC detected during the 40-min drilling simulation was isopropyl alcohol (590 μg/m^3, NIOSH REL = 980,000 μg/m^3). In this study, drilling was performed within one hr of post-processing, where isopropyl alcohol was utilized on the printed part, thereby increasing the likelihood of detection (Freiser et al. 2018).

Yang and Li (2018) established a theoretical model of TVOC emissions during vat printing (SLA-type) with a methyl methacrylate-based feedstock resin and during post-processing of printed parts. They measured the VOCs emitted when the SLA machine was not in operation (reference/background) (10 min), during printing (93 min) and post-process UV-curing and ethanol cleaning of the manufactured part (10 min). The mean TVOC concentrations for the three phases were respectively 123 μg/m^3, 1053 μg/m^3 and 1774 μg/m^3, with a peak concentration of 6177 μg/m^3 during post-processing. Higher TVOC emissions were detected when printing surface area was increased, but that effect was dependent on the type of feedstock resin (Yang and Li 2018).

Väisänen et al. (2019) characterized emissions and IAQ parameters during the printing and post-processing phases for two VP machine and feedstock material combinations (designated as scenario 1 and 2). Scenario 1 involved the manufacture of dental products using a DLP printer and scenario 2 involved the manufacture of miscellaneous parts using an SLA printer. During post-processing, excess

material was removed from the manufactured part surface by washing with isopropanol. In scenario 1, the mean particle number concentration during printing was 8020 ± 1780 #/cm^3 (background: 4420 ± 1620 #/cm^3) with a peak of 13,510 #/cm^3. Dust mass concentrations ranged from below the LOD (MCE filter in IOM sampler) to 120 μg/m^3 (MCE filters used with direct reading instrument) during post-processing (scenario 1). In scenario 2, particle number and mass concentrations were equivalent to background. Only one other study measured particle emissions during VP printing, and that was an environmental test chamber study. Consistent with the results of Väisänen et al. (2019) this chamber study reported that mean particle emissions yields were higher for DLP-type printers compared with SLA-type printers, which indicates that printer technology is an important factor that influences emissions (Stefaniak et al. 2019a).

Gas monitoring by Väisänen et al. (2019) demonstrated that in scenario 1, TVOC concentrations increased at the beginning of the printing phase (peak = 427 μg/m^3) but decreased thereafter to levels lower than the background (< 218 μg/m^3). Among the nine VOCs quantified, methyl methacrylate (27 to 136 μg/m^3), 2-butenoic acid methyl ester (55 to 63 μg/m^3), and 4-methyl-2-pentanone (3 to 76 μg/m^3) were the most prominent. In addition, Väisänen et al. (2019) quantified formaldehyde (12 μg/m^3) and acetone (136 μg/m^3), both of which are classified by NIOSH as potential occupational carcinogens (NIOSH 2007). During post-processing, the TVOC concentration was 1.1 × 10^4 μg/m^3 and 8 VOCs were detected, including 4-methyl-2-pentanone (8139 μg/m^3), isopropanol (1658 μg/m^3), tetrahydro-2-furanylmethyl pivalate (442 μg/m^3), and methyl methacrylate (292 μg/m^3). CO concentrations rose during the printing phase and averaged 0.2 ± 0.3 ppm (range: 0.0 to 1.8 ppm; background mean = 0.0 ± 0.01 ppm), with no changes in CO_2 concentrations. Data suggested that CO was from an external source. For scenario 2, the TVOC concentration was elevated to a maximum of 176 μg/m^3 during the printing phase (background = 55 μg/m^3). The most prominent VOCs were methyl methacrylate (35 to 93 μg/m^3), ethyl methacrylate (14 to 43 μg/m^3), and isopropanol (8 to 24 μg/m^3). Very low concentrations of butanone (22 μg/m^3), acetone (17 μg/m^3), and formaldehyde (3 μg/m^3) were also detected. CO was not detected, and CO_2 levels increased only slightly (510 ± 30 ppm) compared with background (460 ± 60 ppm). Consistent with their TVOC results, an environmental test chamber evaluation of VP printer emissions reported that mean TVOC yields were significantly higher for DLP-type printers compared with SLA-type printers (Stefaniak et al. 2019a).

Zisook et al. (2020) monitored particle and VOC emissions during SLA printing (4.5 hr) using a liquid photopolymer epoxy mixture containing organic compounds and a photoinitiator containing triarylsulfonium salt. No particle emissions data were reported; in a well-ventilated room (129 m^3, ACH = 8.6), emissions were either not detected or described as very low. Fluorine was detected in one of two samples, while antimony was not. TVOC concentrations were not distinguishable from background concentrations during printing. Acetone (mean = 582 μg/m^3) and isopropanol (1377 μg/m^3) were detected during printing at concentrations greater than background; however, Zisook et al. (2020) attributed both compounds to other products used elsewhere in the facility, not from AM machine emissions .

Approaches to monitoring AM process releases and personal exposures

Numerous sampling approaches were used to characterize particle- and gas-phase emissions from AM processes and to assess exposures among workers (Table 2–5). While there are many approaches available, not all samplers are appropriate for all AM processes, which leaves the occupational (industrial) hygienist to question – what is useful? Table 6 summarizes the advantages and limitations of the approaches used for emissions and exposure assessment from the literature summarized in this article. Though this table is focused on workplace measurements, the summary is also applicable to selecting instruments for characterization of emissions for lab toxicology studies. Real-time instruments provided time-resolved data that were useful for understanding fluctuations in concentrations in workplace air; however, most instruments were nonspecific, which necessitated inclusion of time-integrated sampling approaches to characterize the composition of particles and gases using off-line analyses.

Table 5. Summary of gas-phase exposures to additive manufacturing workers.

Room (m^3)	ACH (h^{-1})	Feedstock[a]	Scenario[b]	Sampler[c]	Specifics	Analysis[d]	Substance[e]	C ($\mu g/m^3$)[f]	Cit.[g]
Material extrusion AM process category									
40	NR	ABS, PLA Employee 1	3-DP	Badge	Passive	GC-MS	Acetone	300	A
40	NR	ABS, PLA Employee 1	3-DP/AVP	Badge	Passive	GC-MS	Acetone	6470	
40	NR	ABS, PLA Employee 2	3-DP/AVP	Badge	Passive	GC-MS	Acetone	380	
66	NR	ABS Employee 2	FDM™	Badge	Passive	GC-MS	Acetone	7210	
66	NR	PC Employee 2	FDM™	Badge	Passive	GC-MS	Acetone	2610	
66	NR	ABS, PC Employee 2	FDM™	Badge	Passive	GC-MS	Acetone	290	
Outdoors	N/A	PLA Employee 2	CVP	Badge	Passive	GC-MS	Acetone	4050	
Outdoors	N/A	PLA Employee 2	CVP	Badge	Passive	GC-MS	Chloroform	180	
66	NR	ABS, PC, Ultem®	FDM™	Badge	Passive	GC-MS	Acetone	40–1880	B
				Badge	Passive	GC-MS	Pentane	40–110	
				Badge	Passive	GC-MS	Cyclohexane	10–40	
				Badge	Passive	GC-MS	Ethanol	30–80	
				Badge	Passive	GC-MS	Naphtha	2000–2300	
66	NR	ABS, Ultem®	FDM™	Badge	Passive	GC-MS	Benzene	20–30	
				Badge	Passive	GC-MS	Hexane	150–190	
40	NR	ABS, PLA Employee 1	3-DP (n = 7)	Badge	Passive	GC-MS	Acetone	100	C
				Badge	Passive	GC-MS	Pentane	10	
				Badge	Passive	GC-MS	Ethanol	10	
				Badge	Passive	GC-MS	Naphthas	1450	
40	NR	ABS/PLA Employee 2	3-DP (n = 7)	Badge	Passive	GC-MS	Acetone	50	
				Badge	Passive	GC-MS	Pentane	30	
				Badge	Passive	GC-MS	Hexane	220	
				Badge	Passive	GC-MS	IPA	150	
				Badge	Passive	GC-MS	Naphthas	2090	
40	NR	ABS, PLA Employee 1	3-DP (n = 7)/AVP/Etoh	Badge	Passive	GC-MS	Acetone	2700	
				Badge	Passive	GC-MS	Pentane	150	
				Badge	Passive	GC-MS	Hexane	160	
				Badge	Passive	GC-MS	Ethanol	100	
				Badge	Passive	GC-MS	Naphthas	1330	

(*Continued*)

Table 5. (Continued).

Room (m^3)	ACH (h^{-1})	Feedstock[a]	Scenario[b]	Sampler[c]	Specifics	Analysis[d]	Substance[e]	C ($\mu g/m^3$)[f]	Cit.[g]
40	NR	ABS Employee 2	3-DP	Badge	Passive	GC-MS	Acetone	1880	
				Badge	Passive	GC-MS	Pentane	110	
				Badge	Passive	GC-MS	Hexane	190	
				Badge	Passive	GC-MS	Ethanol	30	
				Badge	Passive	GC-MS	Naphthas	2140	
76	NR	ABS	Printing	Badge	Passive	GC-MS	Acetone	40	
				Badge	Passive	GC-MS	Pentane	40	
				Badge	Passive	GC-MS	IPA	350	
				Badge	Passive	GC-MS	Naphthas	2800	
45	NR	PLA Day 1	3-DP	pPID	10.6 eV	n/a	TVOC	1.4×10^4 (P)	
45	NR	PLA Day 2	3-DP	pPID	10.6 eV	n/a	TVOC	1.8×10^4 (P)	
45	NR	PLA Day 3	3-DP	pPID	10.6 eV	n/a	TVOC	2.9×10^4 (P)	
45	NR	PLA	3-DP	Canister	Evacuated	GC-MS	Acetaldehyde	10–20	
				Canister	Evacuated	GC-MS	Acetone	50–120	
				Canister	Evacuated	GC-MS	Ethanol	40	
				Canister	Evacuated	GC-MS	IPA	2700–9800	
				Canister	Evacuated	GC-MS	MM	2	
Material jetting AM process category									
90	0.22 estimated	TangoBlack+, VeroClear	Printing	Badge	Passive	GC-MS	Acetone	20–80	B
				Badge	Passive	GC-MS	Pentane	10–60	
				Badge	Passive	GC-MS	Ethanol	520–2020	
				Badge	Passive	GC-MS	Naphtha	1530–1710	
				Badge	Passive	GC-MS	IPA	70–520	
Vat photopolymerization AM process category									
NR	NR	White resin	Drilling models	Badge	Passive	GC-MS	IPA	590	D

[a]ABS = acrylonitrile butadiene styrene, PC = polycarbonate, PLA = polylactic acid
[b]3-DP = desktop-scale fused filament fabrication 3D printer, AVP = acetone vapor polishing task, CVP = chloroform vapor polishing task, Etoh = cleaning build platform with ethanol, FDM™ = industrial-scale fused deposition modeling machine
[c]pPID = personal photoionization detector
[d]GC-MS = gas chromatography-mass spectrometry
[e]IPA = isopropyl alcohol, MC = methylene chloride, MM = methyl methacrylate, TVOC = total volatile organic compounds
[f]*P* = peak
[g]A = Du Preez et al. (2018b), B = Stefaniak, Johnson, du Preez, Hammond, Wells, Ham, LeBouf, Martin, et al. (2019b), C = Stefaniak, Johnson, du Preez, Hammond, Wells, Ham, LeBouf, Menchaca, et al. (2019c), D = Freiser et al. (2018)
NR = not reported

Table 6. Advantages and limitations of real-time instruments and time-integrated samplers used to characterize emissions and exposures from additive manufacturing processes.

Approach[a]	Details	Metric(s)	Use[b]	Comment[c]
Real-time particle monitors				
PSM	1 to 3 nm	#/cm^3, size	A	+ Lowest size cutoff among available instruments; used for ME process category − Instrument heavy and delicate which can limit use in workplace studies
F/SMPS	6 to 560 nm	#/cm^3, size	A	+ Lower size cutoff sufficient for PBF, MJ, ME, DED, and BJ processes − Limited portability for field studies; some particles for ME and BJ outside size range
miniDiSC	7 to 400 nm	#/cm^3, size	A, P	+ Lower size cutoff sufficient for PBF, MJ, ME, DED, and BJ processes − Slow response time (~ 7 sec) could underestimate exposure for short duration tasks
EDB	7 to 400 nm	#/cm^3, size	A	+ Lower size cutoff sufficient for PBF, MJ, ME, DED, and BJ processes; good accuracy − Lower size resolution compared with mobility particle sizers
CNC	10 to 1000 nm	#/cm^3	A	+ Hand-held; lower size cutoff sufficient for PBF, MJ, ME, DED, and BJ processes − Wick has finite sampling duration; cannot count smallest particles
DC	10 to 300 nm	#/cm^3, size	A	+ Hand-held; sufficient for PBF, MJ, ME, and DED processes − External "envelope" surface area only
LDSA	10 to 487 nm	#/cm^3, size, μm^2/m^2 lung	A, P	+ Hand-held; particle collection onto TEM grid; sufficient for PBF, MJ, ME, and DED processes − modeled value and generally only accurate in the 10 to 400 nm size range
AMS	30 to 1000 nm	Size, mass	A	+ Chemically resolved particle size and non-refractory mass distribution; used for ME process − Uncertainty with collection efficiency and ionization efficiency for organic aerosols
LSP	0.1 to 15 μm	μg/m^3	A	+ Gives PM_1, $PM_{2.5}$, PM_{10}, and total particle mass concentrations; sufficient for BJ processes − Small particles emitted from PBF, MJ, ME, and DED processes scatter little light (poor signal)
OPS	0.3 to 10 μm	#/cm^3, size, μg/m^3	A	+ Multiple metrics; particle collection onto TEM grid permits microscopic characterization − Many particles from PBF, MJ, ME, and DED processes smaller than lower size cutoff
Time-integrated particle samplers				
Direct-to-substrate[d]	Particles	Shape, size, composition	A	+ Minimizes artifacts from sample handling; chemical information with appropriate detector − Time- and cost-intensive; individual particle analysis might not represent bulk sample
NRD	Particles	<300 nm	A, P	+ Selective for nanoscale particles; successfully used for ME and MJ process categories − Nanoscale particles have little mass; sampler interferences possible (e.g., Ti in membranes)
PVC, TF	Dust	μg/m^3	A, P	+ Simple; inexpensive; multiple sampling heads available for total and size-selective fractions − Gravimetric analysis nonspecific; insensitive for ME, VP, and MJ process categories
PVC, CN	Elements	μg/m^3	A, P	+ Multiple elements; multiple sampling heads available for total and size-selective fractions − Incomplete digestions will underestimate mass; sample interferences possible
QFF	Cr(VI)	μg/m^3	A, P	+ Specific to Cr(VI); multiple sampling heads available for total and size-selective fractions − Impregnated filter needed to prevent redox reactions of Cr compounds before analysis
TEPC	Particles	Shape, size, composition	A, P	+ Smooth surface for SEM analysis; chemical information with appropriate detector − Time- and cost-intensive; individual particle analysis might not represent bulk sample
Real-time gas monitors				
PID	10.6 eV lamp	TVOC	A, P	+ High resolution (1 sec interval) − nonspecific; only measures organic compounds with ionization potential below eV of lamp
Sensor	Various	CO, CO_2, HCN, NH_3, NO_2	A	+ Multiple gases from one instrument − Sample interferences possible from other gases
Sensor	Semiconductor or UV-based	Ozone	A	+ Hand-held; short response time; accurate − Need to select appropriate sensor a priori; slow response time at high concentrations

(*Continued*)

Table 6. (Continued).

Approach[a]	Details	Metric(s)	Use[b]	Comment[c]
Sensor	Electrochemical	Formaldehyde	A	+ Hand-held; specific – Slow response time (8 to 60 sec) could underestimate exposure for short duration tasks
Time-integrated gas samplers				
Badge	Individual VOCs	µg/m^3	A, P	+ Multiple compounds from one sample; no air sampling pump or tubing – Diffusion coefficient must be known for each sampled substance; generally ppm levels
Canister	Individual VOCs	µg/m^3	A, P	+ Whole air sample; multiple compounds from one sample; sensitive; no air sampling pump – Bulky; humidity effects for some VOCs; not amenable for reactive VOCs (e.g., aldehydes)
DNPH	Carbonyls	µg/m^3	A, P	+ Multiple compounds from one sample – Requires reaction with derivitizing agent and formation of stable product until analysis
Impinger	Carbonyls	µg/m^3	A	+ Multiple compounds from one sample – Requires reaction with derivitizing agent and formation of stable product until analysis
TD tube	Individual VOCs	µg/m^3	A, P	+ Many sorbents available to collect a wide range of VOCs; multi-compound analysis – Humidity and storage effects; adsorbent specific to compound or groups of compounds
OE nose	Individual VOCs	Presence	A	+ Many dyes available for identification of VOCs; potential for personal sampling – Time-intensive sample preparation; qualitative results

[a]AMS = aerosol mass spectrometer, CN = cellulose nitrate filters, CNC = condensation nuclei counter (e.g., CPC, *P*-Trak), DC = diffusion charger (e.g., NanoTracer), DNPH = 2,4-Dinitrophenylhydrazine-coated silica gel sorbent tube, EDB = electrometer-based diffusion battery, F/SMPS = fast/scanning mobility particle sizer, LDSA = lung deposited surface area (e.g., NSAM), LSP = laser scattering photometer (e.g., DustTrak™, EPAM), NRD = nanoparticle respiratory deposition sampler, OE nose = optoelectronic nose, OPS = optical particle sizer (e.g., Lighthouse, GRIMM, TSI 3300), PID = photoionization detector, PSM = particle size magnifier, PVC = polyvinyl chloride filter, QFF = quartz fiber filter, TEPC = track-etched polycarbonate filter, TD = thermal desorption tube, TF = Teflon® filter

[b]A = area sampling, *P* = personal breathing zone sampler

[c]BJ = binder jetting process category, Cr = chromium, Cr(VI) = hexavalent chromium, DED = directed energy deposition process category, eV = electron volt, ME = material extrusion process category, MJ = material jetting process category, PBF = powder bed fusion process category, PM_x = particulate matter with aerodynamic diameter less than 1 µm, 2.5 µm, or 10 µm, SEM = scanning electron microscopy, TEM = transmission electron microscopy, Ti = titanium, VOC = volatile organic compound

[d]Direct to substrate = sampling techniques that deposit particles directly onto a substrate for off-line analysis using scanning or transmission microscopy (can include energy dispersive x-ray detector, electron energy loss spectrometry detector, or other detector), attenuated total reflectance Fourier transform infrared spectroscopy (ATR-FTIR), or other characterization technique. Examples include critical orifice with TEM grid (Katz et al. 2020), electrostatic precipitator (ESP) with TEM grid (Mendes et al. 2017; Steinle 2016), mini particle sampler (MPS) with TEM grid (Bau et al. 2020; Jensen et al. 2020; Oberbek et al. 2019; Youn et al. 2019), thermophoretic sampler (TPS) with TEM grid (Dunn, Dunn, et al. 2020a; Gu et al. 2019; Zisook et al. 2020; Zontek et al. 2017), nanometer aerosol sampler (NAS) with TEM grid (Gomes et al. 2019), and single-stage impactors with glass substrate (Zontek et al. 2017)

Real-time particle monitors

Real-time instruments were used for enumeration of airborne particle number, mass, and surface area concentrations and/or determination of size distribution. As presented in Figure 6, a distinguishing feature among these real-time instruments was their particle size measurement range. The size range values depicted in the figure are typical for a type of instrument but might be lower or higher depending on the specific manufacturer, model, and instrument settings. For example, the typical size range of CNC instruments used in most of the reviewed studies was 10 to 1000 nm, though some investigators reported using instruments with measurement ranges of 2.5 to 1000 nm, 4 to 1000 nm, 7 to 1000 nm, 15 to 1000 nm, and 20 to 1000 nm (see Table 2). Figure 6 also shows that sizes of airborne particles reported in the literature reviewed in this article varied among AM process categories because of differences in principles of operation, print parameters, and properties of feedstock materials (no particle size data were reported for VP or SL machines), which indicates that careful selection of particle monitoring instruments is necessary. For example, Mendes et al. (2017) determined particle number concentration from a desktop-scale FFF 3-D printer in a room using a miniDiSC monitor (10 to 700 nm range), CNC (10 to 1000 nm range), SMPS (5 to 350 nm range), and a particle size magnifier (PSM, 1 to 3 nm range). Reported particle number concentrations were 2×10^3 to 4×10^3 #/cm^3 (miniDiSC), 1×10^3 to 3×10^3 #/cm^3 (CNC), 2×10^3 to 9×10^3 #/cm^3 (SMPS), and 10^4 to 10^5 #/cm^3 (PSM). Data demonstrated that a significant

number of 1 to 3 nm particles were detected by the PSM, which means that number-based ERs calculated using mobility sizer or CNC data underestimated actual emissions (Mendes et al. 2017). In another study, it was reported that during FFF 3D printing, particle concentration measurements using an OPS (range: 0.3 to 10 μm) were negligible (i.e., < 0.1%) compared with SMPS measurements (Ding, Wan, and Ng 2020). For personal sampling of particle number concentration and size, the miniDiSC offers the lowest particle-size cutoff. Electrical diffusion batteries (EDB) possess similar lower size cutoffs to the miniDiSC but are larger and relatively heavier, which limits their utility as a personal sampler (Fierz et al 2009). Comparison of reported particle size measurement data in Figure 6 for different AM processes to instrument size measurement ranges yielded the following guidance for monitoring real-time particle number concentration: 1) PSM (1 to 3 nm) was sufficient for ME processes, 2) fast and scanning mobility particle sizes (6 to 560 nm) were sufficient for all five AM process categories with the caveats that smaller particles from ME processes and larger particles from BJ processes will not be counted; 3) miniDiSC (7 to 400 nm), EDB (7 to 400 nm), and CNC (10 to 1000 nm) instruments were sufficient for all AM process categories (with the same caveats as for fast and scanning mobility particle sizer instruments); 4) aerosol mass spectrometer (AMS) instrument (30 to 1000 nm) was employed for an ME process but for MJ and ME processes do not count particles smaller than 30 nm, for BJ machines do not count larger particles, but only measures non-refractory materials such that it is not useful for DED and PBF processes using metallic feedstocks; and, 5) OPS (0.3 to 10 μm) instruments were sufficient for BJ, which released particles with size > 1 μm but not any other AM process category. This guidance has limitations because it was based upon results from instruments selected by investigators in the reviewed literature but may not capture all emissions. For example, PSM data was only reported for the ME process category so it remains unknown whether 1 to 3 nm particles were emitted by other AM process categories.

Real-time determination of particle mass concentration (PM_1, etc.) by LSP instruments (e.g., DustTrak™, Environmental Particulate Air Monitor) is based on total light scattering volume. As shown in Figure 6, many AM process categories emitted particles with diameters of 10s of nm;

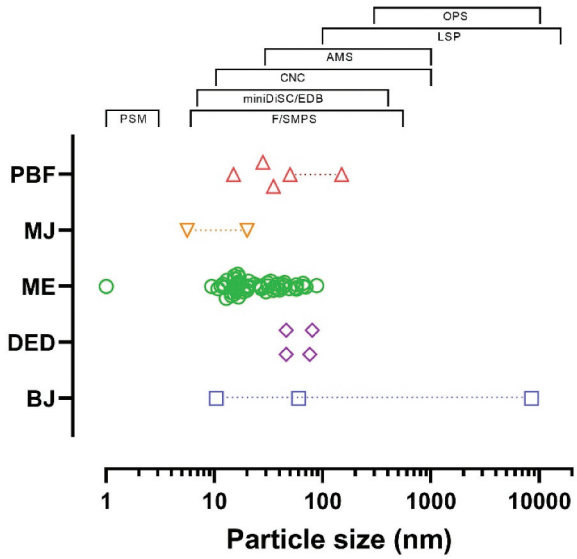

Figure 6. Literature reported particle sizes by additive manufacturing processes category (PBF = powder bed fusion, MJ = material jetting, ME = material extrusion, DED = directed energy deposition, BJ = binder jetting) as well as real-time particle monitoring instrument measurement size ranges. PSM = particle size magnifier (1–3 nm), F/SMPS = fast or scanning mobility particle sizer (6–560 nm), miniDiSC = minidisc monitor (7–400 nm), CNC = condensation nuclei counter (10–1000 nm), AMS = aerosol mass spectrometer (30–1000 nm), LSP = laser scattering photometer (100 nm – 15 μm), OPS = optical particle sizer (300 nm – 20 μm). Dotted lines = range (min-max).

volume is proportional to diameter cubed so these smaller particles will scatter little light. An alternative approach for mass-based measurement of emissions is an AMS, which vaporizes and ionizes particles then measures mass using a time-of-flight mass spectrometer (Katz et al. 2020). This approach relies on analysis of ion fragments, so it is more sensitive than light scattering photometer instruments for nanoscale particles; however, the instrument is less amenable to field measurements compared with photometers and is limited to non-refractory compounds. For monitoring real-time particle mass concentration, LSP (0.1 to 15 μm) instruments may be useful for BJ as this process category emits larger particles but may provide little information for processes (i.e., PBF, MJ, ME, and DED) where emissions are dominated by UFP and/or particles with density near or below 1 g/cm^3 such as many common polymers.

LDSA is a modeled value of particle surface area that deposits in the alveolar region of the lung (Gomes et al. 2019; Stabile et al. 2017). Instruments that report LDSA such as a Nanoparticle Surface Area Monitor use the International Committee on Radiological Protection lung deposition curves for a reference worker and therefore are not representative of a specific individual's exposure. Diffusion chargers (DC) provide an estimate of particle size and surface area (that can be used to model LDSA based on lung deposition curves). Both LDSA and DC instruments are based upon diffusion charging, which might deviate from other measures of surface area for monodisperse particles with sizes greater than approximately a few hundred nanometers (Todea et al. 2017). As such, LDSA (10 to 487 nm) and DC (10 to 300 nm) instruments might provide useful information for PBF, MJ, ME, and DED process categories (with the caveat that emitted particles with size smaller than 10 nm might not be counted) but not BJ processes because LDSA estimates will be inaccurate for larger particles.

Time-integrated particle samplers

Time-integrated particle sampling approaches can provide valuable information on particle morphology, size, and composition. Filter samplers have high versatility because these may be utilized to collect total dust, respirable, thoracic, and inhalable fractions, and other size-selective fractions (Table 6). As noted, nanoscale particles have low volume and many polymer feedstock materials have density of approximately one (e.g., ABS, PLA), which translates to little particle mass. The LOD for mass using a microbalance might be in the microgram range (Fierz et al 2009), which precluded the utility of filter-based gravimetric measurements for the ME, VP, and MJ process categories (Väisänen et al. 2019). Mass spectrometry techniques exhibit lower LODs compared with gravimetric measurements and provide information on specific elements captured on filters and other substrates (Tables 2 and 3). Size-selective sampling down to the nanoscale can be coupled with mass spectrometry analysis to quantify low-levels of elements in workplace air or in the PBZ of workers. Mass spectrometry is a powerful analytical technique because it might be calibrated for simultaneous quantification of multiple elements from the same sample. For example, Some investigators used NRD samplers and quantified low levels of elements in the PBZ of ME and MJ printer operators (Du Preez et al. 2018a; 2018b; Stefaniak et al. 2019b). Respirable and inhalable samplers were used successfully to quantify several metals in emissions and PBZ samples during DED and PBF processes (Bau et al. 2020; Ljunggren et al. 2019; Walter et al. 2018).

Other samplers included direct-to-substrate approaches such as electrostatic and thermophoretic precipitators that collect particles onto an electron microscopy grid, glass slide, or other substrate for off-line analysis by SEM or TEM with little sample preparation. For particles that contain volatile constituents, such as aerosol from ME processes, care should be taken that vacuum conditions and localized sample heating by the electron microscope beam does not volatilize particles or alter particle properties (e.g., size, shape). Some investigators noted that filter-based samples were difficult to analyze by electron microcopy whereas TEM grid samples from a thermophoretic precipitator were amenable to morphological and chemical characterization (Gu et al. 2019; Zisook et al. 2020). Metal particles encountered during PBF processes were highly amenable to electron microscopy characterization (Du Preez et al. 2018a; Mellin et al. 2016).

Real-time gas monitoring

Numerous real-time instruments are available for monitoring gas-phase emissions and exposures. The most widely used real-time gas sampler for AM processes was a PID to determine TVOC concentrations (see Tables 4 and 5). PIDs are rugged and either hand-held or small enough to be attached to a workers clothing; however, they are nonspecific and differences in ionization potential of lamps used in these instruments (usually 10.6 or 11.7 eV) might result in differences in concentration measurements. Further, VOC concentrations measured using PIDs can differ from concentrations measured using GC-MS because PID sensors are sensitive to humidity and interferents might initiate these sensors to under- or overestimate concentrations (Ra et al. 2019). Hence, it is difficult to compare TVOC concentrations measured using a PID amongst studies unless the materials and conditions are identical in workplaces. PIDs are useful for documenting changes in TVOC concentrations relative to background. Alternatively, TVOC levels might also be determined by summing the mass concentration of all individual VOCs collected on tube samplers (described below). As illustrated in Figure 7, a wide range of TVOC concentrations were found for 5 AM process categories, which indicated that this metric was broadly applicable for AM emissions assessments. In general, within a given AM process category, the highest TVOC concentrations were associated with post-processing tasks. Given the upper range of TVOC concentrations reported in the literature, PID instruments are expected to also be useful for AM process categories whereas tube samplers may be subject to breakthrough for high concentrations such as ME and VP post-processing tasks. Numerous sensors were used for real-time monitoring of specific gases, including, but not limited to, hydrogen cyanide, formaldehyde, nitric oxides, CO, CO_2, and ozone. Use of real-time sensors can be especially useful for reactive gases such as aldehydes and ozone which otherwise would need to be stabilized during time-integrated sampling (usually through derivatization). The choice of specific gas sensor must be tailored to the anticipated process emissions for a given combination of AM process category and feedstock material. For example, Davis et al. (2019) observed in an environmental test chamber study that ME-type FFF 3-D printing with nylon filament released formaldehyde so real-time monitoring for this substance may be conducted for processes that use nylon feedstock materials such as ME or PBF.

Time-integrated gas samplers

A variety of time-integrated sampling approaches were used for gas-phase contaminants, including passive badges, evacuated canisters, impingers, an optoelectronic nose, and tubes with myriad adsorbents. The main advantage of most time-integrated sampling techniques for gases is that they may be

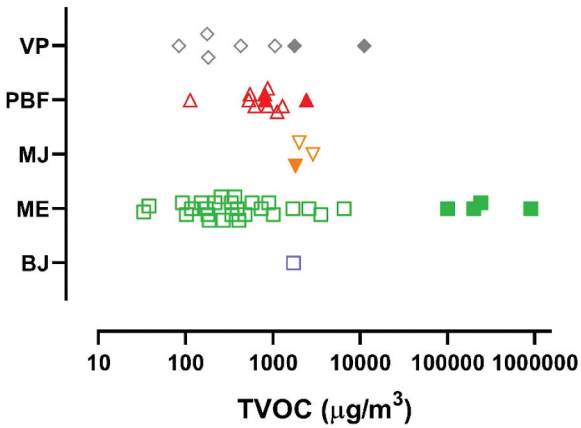

Figure 7. Real-time total volatile organic compound (TVOC) concentrations measured using a photoionization detector (10.6 eV lamp) by additive manufacturing processes category (VP = vat photopolymerization, PBF = powder bed fusion, MJ = material jetting, ME = material extrusion, BJ = binder jetting). Data reported as either concentration, concentration range or peak concentration. Open symbols = pre-printing and printing/processing, Filled symbols = post processing.

used for area air monitoring and personal exposure monitoring of specific chemical substances. Each time-integrated gas sampling approach given in Table 6 has its relative advantages and limitations. For example, passive badges do not use a sampling pump to draw air across the sampling media, which could be advantageous in some workplaces; however, diffusion coefficients in the badge media need to be known for each analyte. The choice of sampling method is dependent upon the anticipated gas-phase contaminants to be released for a given combination of AM process category and feedstock material. Note that even within an AM process category, gas-phase emissions may vary from the same machine using different feedstock materials. Numerous standard sampling and analytical methods for specific gas-phase contaminants are available from the U.S. Environmental Protection Agency (Hazardous Waste Test Methods/SW-846 | US EPA) (EPA EPA 2021), U.S. Occupational Safety and Health Administration (Sampling and Analytical Methods | Occupational Safety and Health Administration (osha.gov)) (DOL 2021), U.S. National Institute for Occupational Safety and Health (CDC – NIOSH Publications and Products – NIOSH Manual of Analytical Methods (2014–151)) (NIOSH NIOSH Manual of Analytical Methods (NMAM) 2021), and organizations such as ASTM International (Committee D22 on Air Quality – Published standards under D22 jurisdiction (astm.org)) (ASTM International 2021). The correct air sample collection media and analytical technique will vary depending upon the analyte of interest, expected environmental conditions during sampling, and capabilities of the laboratory or researcher. Among available analytical techniques, GC-MS is a powerful tool because it can be calibrated for simultaneous quantification of multiple compounds from the same sample. Further, standard mass spectra databases exist, which permit matching of sample spectra for qualitative identification of sample constituents. This latter advantage is especially useful for identification of byproducts formed by thermal degradation of feedstock, which might not be known prior to sampling. Further, some SDS do not report all possible product constituents (LeBouf, Hawley, and Cummings 2019), which makes it difficult to design a targeted emission and/or exposure assessment strategy when analytes are unknown. Time-integrated sampling approaches for organic and inorganic gases are useful for assessments of AM process categories that utilize polymer feedstock materials (i.e., all but DED and PBF with metals).

Research gaps and needs

Available literature has increased our understanding of workplace emissions and exposures from AM processes during the last 8 years (Figure 2); however, AM is dynamic and constantly evolving. New machine designs and innovations and new feedstock materials present challenges for occupational (industrial) hygienists to ensure appropriate health and safety conditions for workers and for toxicologists to design studies that accurately mimic exposures encountered in real-world conditions. At present, there is not one instrument capable of simultaneous real-time monitoring and characterization measurements that is appropriate for all AM process categories. Building on the literature reviewed herein, we suggest the following areas for future research (no prioritization is implied by the order of the list) for occupational hygienists and toxicologists:

- Improve understanding of factors that influence emissions and exposures in real-world settings
- Include all seven AM process categories (currently no data are available for SL processes)
- Evaluate AM facility- or workspace-related factors
- Ventilation (general ventilation, HVAC systems, local exhaust ventilation, etc.) and effectiveness thereof
- Evaluate AM machine-related factors
- Machine design (sealed, filters, built-in ventilation, etc.) and operating configurations (doors open/closed, etc.)
- Evaluate feedstock-related factors
- Formulations (constituents, especially those not declared on SDSs)
- Additives (engineered nanomaterials, colorants, plasticizers, flame retardants, esthetic, and functional materials)

- Recycled powders and polymers compared with virgin feedstocks
- Expand exposure assessments to include the dermal exposure pathway and biological markers of exposure, where available
- Develop predictive models for rating emissions from bulk characteristics of feedstock materials to inform users
- Perform more field assessments to understand which tasks contribute most to exposures throughout an AM process (pre-printing, printing, post-printing, and post-processing)
- Develop internationally harmonized methods for workplace assessments of emissions and exposures and data reporting that include relevant particle metrics (number count and surface area for processes such as ME that predominantly emit UFP and mass for processes such as BJ that emit micron-scale particles) and volatile organic and SVOC compound monitoring approaches for all but metal-based processes
- Promote prevention-through-design concepts in machine design and operator training to reduce emissions and exposures
- Develop real-time instruments that are sufficiently sensitive and portable to measure substance-specific mass ERs
- Evaluate emissions and exposures from multiple types of AM process categories operating simultaneously in the same space for additive or synergistic effects.

Acknowledgments

The authors thank Dr. S. Linde (North-West University) and Dr. J.R. Wells (NIOSH) for critical review of this manuscript prior to submission to the journal. The findings and conclusions in this report are those of the authors and do not necessarily represent the official position of the National Institute for Occupational Safety and Health, Centers for Disease Control and Prevention. Mention of any company or product does not constitute endorsement by the U.S. Government, National Institute for Occupational Safety and Health, or Centers for Disease Control and Prevention. This work was supported by NIOSH intramural research funds and The South African Department of Science and Innovation through the Competitive Programme in Additive Manufacturing.

Funding

This work was supported by the Department of Science and Innovation, South Africa [Competitive Programme in Additive Manufacturing]; NIOSH intramural funds.

Declaration of statement

The authors declare they have no conflict of interests.

Data availability statement

There is no data set associated with this paper.

References

Afshar-Mohajer, N., C. Y. Wu, T. Ladun, D. A. Rajon, and Y. Huang. 2015. Characterization of particulate matters and total VOC emissions from a binder jetting 3D printer. *Build. Environ.* 93:293–301. doi:10.1016/j.buildenv.2015.07.013.

Alberts, E., M. Ballentine, E. Barnes, and A. Kennedy. 2021. Impact of metal additives on particle emission profiles from a fused filament fabrication 3D printer. *Atmos. Environ.* 244:117956. Article. doi:10.1016/j.atmosenv.2020.117956.

Aluri, M., B. Monami, B. S. Raj, and R. S. Mamilla. 2021. Review on particle emissions during fused deposition modeling of acrylonitrile butadiene styrene and polylactic acid polymers. *Materials Today: Proceedings* (E-print).

ASTM International, *Standards under the jurisdiction of D22*. ASTM International 2021 [cited February 2, 2021]. Available from https://www.astm.org/COMMIT/SUBCOMMIT/D22.htm

Bau, S., D. Rousset, R. Payet, and F. X. Keller. 2020. Characterizing particle emissions from a direct energy deposition additive manufacturing process and associated occupational exposure to airborne particles. *J Occup Environ Hyg* 17 (2–3):59–72. doi:10.1080/15459624.2019.1696969.

Beisser, R., M. Buxtrup, D. Fendler, L. Hohenberger, V. Kazda, Y. Von Mering, H. Niemann, K. Pitzke, and R. Weiß. 2017. Inhalation exposure to metals during additive processes (3D printing). *Gefahrstoffe Reinhaltung der Luft* 77:487–96.

Bernatikova, S., A. Dudacec, R. Prichystalova, V. Klecka, and L. Kocurkova. 2021. Characterization of ultrafine particles and VOCs emitted from a 3D printer. *Int J Environ Res Public Health* Article. 18 (3):929. doi:10.3390/ijerph18030929.

Bharti, N., and S. Singh. 2017. Three-dimensional (3D) printers in libraries: Perspective and preliminary safety analysis. *J. Chem. Educ.* 94 (7):879–85. doi:10.1021/acs.jchemed.6b00745.

Bourell, D. L. 2016. Perspectives on additive manufacturing. *Annu Rev Mater Res* 46 (1):1–18. doi:10.1146/annurev-matsci-070115-031606.

Bours, J., B. Adzima, S. Gladwin, J. Cabral, and S. Mau. 2017. Addressing hazardous implications of additive manufacturing: Complementing life cycle assessment with a framework for evaluating direct human health and environmental impacts. *Journal of Industrial Ecology* 21 (S1):S25–S36. doi:10.1111/jiec.12587.

Bravi, L., F. Murmura, and G. Santos. 2019. Additive manufacturing: Possible problems with indoor air quality. *Procedia Manufacturing* 41:952–59. doi:10.1016/j.promfg.2019.10.020.

Chan, F. L., C. Y. Hon, S. M. Tarlo, N. Rajaram, and R. House. 2020. Emissions and health risks from the use of 3D printers in an occupational setting. *J. Toxicol. Environ. Health Part A* 83 (7):279–87. doi:10.1080/15287394.2020.1751758.

Chang, T. Y., L. J. Lee, J. D. Wang, R. H. Shie, and C. C. Chan. 2004. Occupational risk assessment on allergic contact dermatitis in a resin model making process. *Journal of Occuppational Health* 46 (2):148–52. doi:10.1539/joh.46.148.

Chen, R., H. Yin, I. S. Cole, S. Shen, X. Zhou, Y. Wang, and S. Tang. 2020. Exposure, assessment and health hazards of particulate matter in metal additive manufacturing: A review. *Chemosphere* 259:127452. Article. doi:10.1016/j.chemosphere.2020.127452.

Chýlek, R., L. Kudela, J. Pospíšil, and L. Šnajdárek. 2019. Fine particle emission during fused deposition modelling and thermogravimetric analysis for various filaments. *J. Clean. Prod.* 237:117790. Article. doi:10.1016/j.jclepro.2019.117790.

Damanhuri, A. A. M., A. Hariri, M. R. Alkahari, M. H. F. M. Fauadi, and S. F. Z. Bakri. 2019a. Indoor air concentration from selective laser sintering 3D printer using virgin polyamide nylon (PA12) powder: A pilot study. *International Journal of Integrated Engineering* 11 (5 Special):140–49.

Damanhuri, A. A. M., A. S. A. Subki, A. Hariri, B. T. Tee, M. H. F. M. Fauadi, M. S. F. Hussin, and M. S. S. Mustafa. 2019b. Comparative study of selected indoor concentration from selective laser sintering process using virgin and recycled polyamide nylon (PA12). *IOP Conference Series: Earth and Environmental Science* 373 Article 012014, Malacca, Malaysia.

Davis, A. Y., Q. Zhang, J. P. S. Wong, R. J. Weber, and M. S. Black. 2019. Characterization of volatile organic compound emissions from consumer level material extrusion 3D printers. *Build. Environ.* 160:106209. Article. doi:10.1016/j.buildenv.2019.106209.

Deak, S. M. 1999. Safe work practices for rapid prototyping. *Rapid Prototyping Journal* 5 (4):161–63. doi:10.1108/13552549910295479.

Deng, Y., S. J. Cao, A. Chen, and Y. Guo. 2016. The impact of manufacturing parameters on submicron particle emissions from a desktop 3D printer in the perspective of emission reduction. *Build. Environ.* 104:311–19. doi:10.1016/j.buildenv.2016.05.021.

Ding, S., B. F. Ng, X. Shang, H. Liu, X. Lu, and M. P. Wan. 2019. The characteristics and formation mechanisms of emissions from thermal decomposition of 3D printer polymer filaments. *Science of the Total Environment* 692:984–94. doi:10.1016/j.scitotenv.2019.07.257.

Ding, S., M. P. Wan, and B. F. Ng. 2020. Dynamic analysis of particle emissions from FDM 3D printers through a comparative study of chamber and flow tunnel measurements. *Environ. Sci. Technol.* 54 (22):14568–77. doi:10.1021/acs.est.0c05309.

DOL. *Sampling and Analytical Methods*. Directorate of Technical Support and Emergency Management/Salt Lake Technical Center [cited February 2, 2021]. Available from https://www.osha.gov/dts/sltc/methods/index.html

Du Preez, S., A. Johnson, R. F. LeBouf, S. J. L. Linde, A. B. Stefaniak, and J. Du Plessis. 2018b. Exposures during industrial 3-D printing and post-processing tasks. *Rapid Prototyping Journal* 24 (5):865–71. doi:10.1108/RPJ-03-2017-0050.

Du Preez, S., D. J. de Beer, and J. L. Du Plessis. 2018a. Titanium powders used in powder bed fusion: Their relevance to respiratory health. *South African Journal of Industrial Engineering* 29 (4):94–102. doi:10.7166/29-4-1975.

Dunn, K. L., D. Hammond, K. Menchaca, G. Roth, and K. H. Dunn. 2020b. Reducing ultrafine particulate emission from multiple 3D printers in an office environment using a prototype engineering control. *Journal of Nanoparticle Research* Article. 22 (5):112. doi:10.1007/s11051-020-04844-4.

Dunn, K. L., K. H. Dunn, D. Hammond, and S. Lo. 2020a. Three-dimensional printer emissions and employee exposures to ultrafine particles during the printing of thermoplastic filaments containing carbon nanotubes or carbon nanofibers. *Journal of Nanoparticle Research* Article. 22 (2):46. doi:10.1007/s11051-020-4750-8.

Elder, A., and G. Oberdörster. 2006. Translocation and effects of ultrafine particles outside of the lung. *Clin Occup Environ Med* 5 (4):785–96. doi:10.1016/j.coem.2006.07.003.

EPA. *SW-846: Test Methods for Evaluating Solid Waste: Physical/Chemical Methods*. US EPA Office of Solid Waste; Economic, Methods, and Risk Analysis Division 2014 [cited February 2, 2021]. Available from https://www.epa.gov/hw-sw846

Fierz, M., A. Keller, and H. Burtscher. 2009. Charge-based personal aerosol samplers. *Inhal Toxicol* 21 (Suppl sup1):30–34. doi:10.1080/08958370902942632.

Fierz, M., S. Weimer, and H. Burtscher. 2009. Design and performance of an optimized electrical diffusion battery. *J Aerosol Sci* 40 (2):152–63. doi:10.1016/j.jaerosci.2008.09.007.

Ford, S. 2014. Additive Manufacturing technology: Potential implications for U.S. manufacturing competitiveness. *Journal of International Commerce and Economics*. http://www.usitc.gov/journals .

Freiser, M. E., A. Ghodadra, L. Hart, C. Griffith, and N. Jabbour. 2018. Safety of drilling 3-dimensional-printed temporal bones. *Otolaryngology-Head & Neck Surgery* 144:797–801.

Gomes, J. F., R. M. Miranda, J. P. Oliveira, H. M. Esteves, and P. C. Albuquerque. 2019. Evaluation of the amount of nanoparticles emitted in LASER additive manufacture/welding. *Inhal Toxicol* 31 (3):125–30. doi:10.1080/08958378.2019.1621965.

Graff, P., B. Ståhlbom, E. Nordenberg, A. Graichen, P. Johansson, and H. Karlsson. 2017. Evaluating measuring techniques for occupational exposure during additive manufacturing of metals: A pilot study. *Journal of Industrial Ecology* 21 (S1):S120–S129. doi:10.1111/jiec.12498.

Gu, J., M. Wensing, E. Uhde, and T. Salthammer. 2019. Characterization of particulate and gaseous pollutants emitted during operation of a desktop 3D printer. *Environmental International* 123:476–85. doi:10.1016/j.envint.2018.12.014.

He, C., L. Morawska, and L. Taplin. 2007. Particle emission characteristics of office printers. *Environmental Science & Technology* 41 (17):6039–45. doi:10.1021/es063049z.

ISO/ASTM. 2015. *52900: Additive manufacturing — General principles — Terminology Geneva*. Switzerland: ISO.

Ivanova, O., C. Williams, and T. Campbell. 2013. Additive manufacturing (AM) and nanotechnology: Promises and challenges. *Rapid Prototyping Journal* 19 (5):353–64. doi:10.1108/RPJ-12-2011-0127.

Jensen, A. C. O., H. Harboe, A. Brostrøm, K. A. Jensen, and A. S. Fonseca. 2020. Nanoparticle exposure and workplace measurements during processes related to 3D printing of a metal object. *Frontiers in Public Health* 8 (Article):608718. doi:10.3389/fpubh.2020.608718.

Katz, E. F., J. D. Goetz, C. Wang, J. L. Hart, B. Terranova, M. L. Taheri, M. S. Waring, and P. F. DeCarlo. 2020. Chemical and physical characterization of 3D printer aerosol emissions with and without a filter attachment. *Environmental Science & Technology* 54 (2):947–54. doi:10.1021/acs.est.9b04012.

Kolb, T., P. Schmidt, R. Beisser, J. Tremel, and M. Schmidt. 2017. Safety in additive manufacturing: Fine dust measurements for a process chain in laser beam melting of metals. *RTeJournal: Fachforum Fur Rapid Technologie*2017.

LeBouf, R. F., B. Hawley, and K. J. Cummings. 2019. Potential hazards not communicated in safety data sheets of flavoring formulations, including diacetyl and 2,3-pentanedione. *Annals of Work Exposure and Health* 63 (1):124–30. doi:10.1093/annweh/wxy093.

Leso, V., M. L. Ercolano, I. Mazzotta, M. Romano, F. Cannavacciuolo, and I. Iavicoli. 2021. Three-dimensional (3D) printing: Implications for risk assessment and management in occupational settings. *Annals of Work Exposure and Health (E-print)*. doi:10.1093/annweh/wxaa146.

Lewinski, N. A., L. E. Secondo, and J. K. Ferri. 2019. On-site three-dimensional printer aerosol hazard assessment: Pilot study of a portable in vitro exposure cassette. *Process Safety Progress* 38 (3), 6. doi: 10.1002/prs.12030.

Ljunggren, S. A., H. Karlsson, B. Ståhlbom, B. Krapi, L. Fornander, L. E. Karlsson, B. Bergström, E. Nordenberg, T. K. Ervik, and P. Graff. 2019. Biomonitoring of Metal Exposure During Additive Manufacturing (3D Printing). *Saf Health Work* 10 (4):518–26. doi:10.1016/j.shaw.2019.07.006.

Ma, X., J. Liu, W. Zhu, M. Tang, N. Lawrence, C. Yu, M. Gou, and S. Chen. 2018. 3D bioprinting of functional tissue models for personalized drug screening and in vitro disease modeling. *Adv. Drug Deliv. Rev.* 132:235–51. doi:10.1016/j.addr.2018.06.011.

McDonnell, B., X. J. Guzman, M. Dolack, T. W. Simpson, and J. M. Cimbala. 2016. 3D printing in the wild: A preliminary investigation of air quality in college maker spaces. Paper read at Solid Freeform Fabrication 2016 – An Additive Manufacturing Conference, at Austin, TX.

Mellin, P., C. Jönsson, M. Åkermo, P. Fernberg, E. Nordenberg, H. Brodin, and A. Strondl. 2016. Nano-sized by-products from metal 3D printing, composite manufacturing and fabric production. *J. Clean. Prod.* 139:1224–33. doi:10.1016/j.jclepro.2016.08.141.

Mendes, L., A. Kangas, K. Kukko, B. Mølgaard, A. Säämänen, T. Kanerva, I. Flores Ituarte, M. Huhtiniemi, H. Stockmann-Juvala, J. Partanen, et al.. 2017. Characterization of emissions from a desktop 3D printer. *Journal of Industrial Ecology* 21 (S1):S94–S106. doi:10.1111/jiec.12569.

Nagarajan, H. P. N., S. Panicker, H. Mokhtarian, E. Coatanéa, and K. R. Haapala. 2020. Improving worker health and safety in wire arc additive manufacturing: A graph-based approach. *Procedia CIRP* 90:461–66. doi:10.1016/j.procir.2020.01.116.

NIOSH. 2007. *NIOSH Pocket Guide to Chemical Hazards*. In *DHHS (NIOSH) Publication 2005-149 ed*, Cincinnati, OH: DHHS (NIOSH). [Cited February 2, 2021]. Available from https://www.cdc.gov/niosh/npg/default.html

NIOSH Manual of Analytical Methods (NMAM), 5th Edition U.S. Department of Health and Human Services, Centers for Disease Control and Prevention, National Institute for Occupational Safety and Health 2020 [cited February 2, 2021]. Available from https://www.cdc.gov/niosh/nmam/default.html

Oberbek, P., P. Kozikowski, K. Czarnecka, P. Sobiech, S. Jakubiak, and T. Jankowski. 2019. Inhalation exposure to various nanoparticles in work environment—contextual information and results of measurements. *Journal of Nanoparticle Research* Article. 21 (11):222. doi:10.1007/s11051-019-4651-x.

Pelley, J. 2018. Safety Standards Aim to Rein in 3-D Printer Emissions. *ACS Central Science* 4 (2):134–36. doi:10.1021/acscentsci.8b00090.

Petretta, M., G. Desando, B. Grigolo, and L. Roseti. 2019. 3D printing of musculoskeletal tissues: Impact on safety and health at work. *Journal of Toxicology and Environmental*

Health A 82 (16):891–912. doi:10.1080/15287394.2019.1663458.

Philippot, C., C. L'Allain, S. Artous, D. Locatelli, S. Jacquinot, S. Derrough, L. Aixala, P. Mougenel, and Y. Gallet. 2020. Potential workers exposure measurement in metal additive manufacturing and how to manage it. *Proceedings of Euro Powder Metallurgy, Bilbao, Spain*.

Pinheiro, N. D., R. T. Freire, J. Aparecida, M. Conrado, A. D. Batista, and J. F. Da S Petruci. 2021. Paper-based optoelectronic nose for identification of indoor air pollution caused by 3D printing thermoplastic filaments. *Anal. Chim. Acta* 1143:1–8. doi:10.1016/j.aca.2020.11.012.

Potter, P. M., S. R. Al-Abed, D. Lay, and S. M. Lomnicki. 2019. VOC emissions and formation mechanisms from carbon nanotube composites during 3D printing. *Environ. Sci. Technol.* 53 (8):4364–70. doi:10.1021/acs.est.9b00765.

Ra, K., S. M. Teimouri Sendesi, M. Nuruddin, N. N. Zyaykina, E. N. Conkling, B. E. Boor, C. T. Jafvert, J. A. Howarter, J. P. Youngblood, and A. J. Whelton. 2019. Considerations for emission monitoring and liner analysis of thermally manufactured sewer cured-in-place-pipes (CIPP). *J. Hazard. Mater.* 371:540–49. doi:10.1016/j.jhazmat.2019.02.097.

Roth, G. A., C. L. Geraci, A. Stefaniak, V. Murashov, and J. Howard. 2019. Potential occupational hazards of additive manufacturing. *J Occup Environ Hyg* 16 (5):321–28. doi:10.1080/15459624.2019.1591627.

Ryan, T., and D. Hubbard. 2016. 3-D printing hazards: Literature review & preliminary hazard assessment. *Prof Saf* 61:56–62.

Shahin-Shamsabadi, A., and P. R. Selvaganapathy. 2019. ExCeL: Combining extrusion printing on cellulose scaffolds with lamination to create in vitro biological models. *Biofabrication* Article. 11 (3):035002. doi:10.1088/1758-5090/ab0798.

Short, D. B., A. Sirinterlikci, P. Badger, and B. Artieri. 2015. Environmental, health, and safety issues in rapid prototyping. *Rapid Prototyping Journal* 21 (1):105–10. doi:10.1108/RPJ-11-2012-0111.

Simon, T. R., G. A. Aguilera, and F. Zhao. 2017. Characterization of particle emission from fuse deposition modeling printers. Paper read at Proceedings of the ASME 2017 12th International Manufacturing Science and Engineering Conference, Los Angeles, CA.

Sousa, M., P. Arezes, and F. Silva. 2019. Nanomaterials exposure as an occupational risk in metal additive manufacturing. *Journal of Physics: Conference Series* 1323 Article 012013, Minatec-Grenoble, France.

Stabile, L., M. Scungio, G. Buonanno, F. Arpino, and G. Ficco. 2017. Airborne particle emission of a commercial 3D printer: The effect of filament material and printing temperature. *Indoor Air* 27 (2):398–408. doi:10.1111/ina.12310.

Stefaniak, A. B., A. R. Johnson, S. Du Preez, D. R. Hammond, J. R. Wells, J. E. Ham, R. F. LeBouf, K. W. Menchaca, S. B. Martin Jr., M. G. Duling, et al.. 2019c. Evaluation of emissions and exposures at workplaces using desktop 3-dimensional printers. *Journal of Chemical Health and Safety* 26 (2):19–30. doi:10.1016/j.jchas.2018.11.001.

Stefaniak, A. B., A. R. Johnson, S. Du Preez, D. R. Hammond, J. R. Wells, J. E. Ham, R. F. LeBouf, S. B. Martin Jr., M. G. Duling, L. N. Bowers, et al.. 2019b. Insights into emissions and exposures from use of industrial-scale additive manufacturing machines. *Saf Health Work* 10 (2):229–36. doi:10.1016/j.shaw.2018.10.003.

Stefaniak, A. B., L. N. Bowers, A. K. Knepp, M. A. Virji, E. M. Birch, J. E. Ham, J. R. Wells, C. Qi, D. Schwegler-Berry, S. Friend, et al.. 2018. Three-dimensional printing with nano-enabled filaments releases polymer particles containing carbon nanotubes into air. *Indoor Air* 28 (6):840–51. doi:10.1111/ina.12499.

Stefaniak, A. B., L. N. Bowers, A. K. Knepp, T. P. Luxton, D. M. Peloquin, E. J. Baumann, J. E. Ham, J. R. Wells, A. R. Johnson, R. F. LeBouf, et al.. 2019a. Particle and vapor emissions from vat polymerization desktop-scale 3-dimensional printers. *J Occup Environ Hyg* 16 (8):519–31. doi:10.1080/15459624.2019.1612068.

Steinle, P. 2016. Characterization of emissions from a desktop 3D printer and indoor air measurements in office settings. *J Occup Environ Hyg* 13 (2):121–32. doi:10.1080/15459624.2015.1091957.

Stephens, B., P. Azimi, Z. El Orch, and T. Ramos. 2013. Ultrafine particle emissions from desktop 3D printers. *Atmos. Environ.* 79:334–39. doi:10.1016/j.atmosenv.2013.06.050.

Sutton, A. T., C. S. Kriewall, S. Karnati, M. C. Leu, and J. W. Newkirk. 2020. Characterization of AISI 304L stainless steel powder recycled in the laser powder-bed fusion process. *Additive Manufacturing* 32 (Article):100981. doi:10.1016/j.addma.2019.100981.

Todea, A. M., S. Beckmann, H. Kaminski, D. Bard, S. Bau, S. Clavaguera, D. Dahmann, H. Dozol, N. Dziurowitz, K. Elihn, et al.. 2017. Inter-comparison of personal monitors for nanoparticles exposure at workplaces and in the environment. *Science of the Total Environment* 605-606:929–45. doi:10.1016/j.scitotenv.2017.06.041.

Väisänen, A. J. K., M. Hyttinen, S. Ylönen, and L. Alonen. 2019. Occupational exposure to gaseous and particulate contaminants originating from additive manufacturing of liquid, powdered, and filament plastic materials and related post-processes. *J Occup Environ Hyg* 16 (3):258–71. doi:10.1080/15459624.2018.1557784.

Vance, M. E., V. Pegues, S. Van Montfrans, W. Leng, and L. C. Marr. 2017. Aerosol emissions from fuse-deposition modeling 3D printers in a chamber and in real indoor environments. *Environmental Science & Technology* 51 (17):9516–23. doi:10.1021/acs.est.7b01546.

Walter, J., A. Baumgärtel, M. Hustedt, R. Hebisch, and S. Kaierle. 2018. Inhalation exposure to hazardous substances during powder-bed processes. *Procedia CIRP* 74:295–99. doi:10.1016/j.procir.2018.08.114.

Wei, Z., X. Liu, M. Ooka, L. Zhang, M. J. Song, R. Huang, N. C. Kleinstreuer, A. Simeonov, M. Xia, and M. Ferrer.

2020. Two-dimensional cellular and three-dimensional bio-printed skin models to screen topical-use compounds for irritation potential. *Frontiers in Bioengineering Biotechnology* 8:109. 8 Article. doi:10.3389/fbioe.2020.00109.

Wojtyła, S., P. Klama, K. Śpiewak, and T. Baran. 2020. 3D printer as a potential source of indoor air pollution. *International Journal of Environmental Science and Technology* 17 (1):207–18. doi:10.1007/s13762-019-02444-x.

Wu, H., W. P. Fahy, S. Kim, H. Kim, N. Zhao, L. Pilato, A. Kafi, S. Bateman, and J. H. Koo. 2020. Recent developments in polymers/polymer nanocomposites for additive manufacturing. *Prog Mater Sci* 111:1–47. doi:10.1016/j.pmatsci.2020.100638.

Yang, Y., and L. Li. 2018. Total volatile organic compound emission evaluation and control for stereolithography additive manufacturing process. *J. Clean. Prod.* 170:1268–78. doi:10.1016/j.jclepro.2017.09.193.

Yi, J., R. F. LeBouf, M. G. Duling, T. R. Nurkiewicz, B. T. Chen, D. Schwegler-Berry, M. A. Virji, and A. B. Stefaniak. 2016. Emission of particulate matter from a desktop three-dimensional (3-D) printer. *Journal of Toxicology and Environmental Health A* 79 (11):453–65. doi:10.1080/15287394.2016.1166467.

Youn, J. S., J. W. Seo, S. Han, and K. J. Jeon. 2019. Characteristics of nanoparticle formation and hazardous air pollutants emitted by 3D printer operations: From emission to inhalation. *RSC Adv* 9 (34):19606–12. doi:10.1039/C9RA03248G.

Zhang, Y., W. Jarosinski, Y.-G. Jung, and J. Zhang. 2018. 2 - Additive manufacturing processes and equipment. In *Additive Manufacturing*, ed. J. Zhang, and Y.-G. Jung. (pp. 39-51). Butterworth-
Heineman, Oxford, United Kingdom.

Zhou, Y., X. Kong, A. Chen, and S. Cao. 2015. Investigation of ultrafine particle emissions of desktop 3D printers in the clean room. *Procedia Engineering* 121:506–12. doi:10.1016/j.proeng.2015.08.1099.

Zisook, R. E., B. D. Simmons, M. Vater, A. Perez, E. P. Donovan, D. J. Paustenbach, and W. D. Cyrs. 2020. Emissions associated with operations of four different additive manufacturing or 3D printing technologies. *J Occup Environ Hyg* 17 (10):464–79. doi:10.1080/15459624.2020.1798012.

Zontek, T. L., B. R. Ogle, J. T. Jankovic, and S. M. Hollenbeck. 2017. An exposure assessment of desktop 3D printing. *Journal of Chemical Health and Safety* 24 (2):15–25. doi:10.1016/j.jchas.2016.05.008.

Zontek, T. L., S. Hollenbeck, J. Jankovic, and B. R. Ogle. 2019. Modeling particle emissions from three-dimensional printing with acrylonitrile-butadiene-styrene polymer filament. *Environ. Sci. Technol.* 53 (16):9656–63. doi:10.1021/acs.est.9b02818.